THESIS FOR THE DEGREE OF LICENTIATE OF ENGINEERING

Beamforming Strategies for In-Band Full-Duplex Wireless Systems

Mustafa Ayebe

CHALMERS
UNIVERSITY OF TECHNOLOGY

Antenna Systems Group
Department of Electrical Engineering
Chalmers University of Technology
Gothenburg, Sweden, 2025

Beamforming Strategies for In-Band Full-Duplex Wireless Systems

Mustafa Ayebe

Department of Electrical Engineering
Chalmers University of Technology
SE-412 96 Gothenburg, Sweden
Phone: +46 (0)31 772 1000
www.chalmers.se

Printed by Chalmers Reproservice
Gothenburg, Sweden, May 2025

Her daim yanımda olan aileme ithafen.

Abstract

In-band full-duplex (IBFD) wireless communication promises to revolutionize future wireless systems by enabling simultaneous transmission and reception over the same frequency band, effectively doubling spectral efficiency. However, its practical implementation is challenged by strong self-interference (SI) from the transmitter to the receiver, which can saturate the receiver front-end and degrade overall system performance. While various SI cancellation techniques have been developed across the propagation, analog, and digital domains, they are often categorized based on the domain in which cancellation occurs. This domain-specific design approach can limit scalability and robustness, especially in antenna array-based systems.

This thesis addresses these limitations through a novel joint transmit-receive (Tx-Rx) beamforming framework specifically designed for IBFD antenna arrays. Unlike conventional methods that treat Tx and Rx beamforming separately, the proposed strategy jointly optimizes both to maximize antenna gain while maintaining SI below a critical threshold level. The constraints on the Tx-side ensure the receiver operates in its linear regime, while the Rx-side optimization further suppresses residual SI to enhance the signal-to-self-interference ratio and support reliable reception.

The framework is built upon electromagnetic modeling based on scattering parameters and embedded element patterns, and incorporates newly defined figures of merit to evaluate system-level isolation and performance trade-offs. A systematic optimization strategy is developed, and its effectiveness is demonstrated through full-wave simulations of a dual-aperture IBFD array using Method of Moments analysis. Key insights into beamforming flexibility, frequency selectivity, and isolation vs. gain trade-offs are revealed through eigenvalue analysis and pattern shaping studies.

To validate the proposed concept, an integrated IBFD testbed was developed using 3D-printed, silver-coated Vivaldi arrays operating in the $3-6$ GHz band, together with the Zynq UltraScale+ RFSoC ZCU216 platform. Measurements closely match simulation results despite practical hardware impairments such as DAC/ADC nonlinearities. With a conventional Tx maximum-gain beamformer, the measured isolation between the closely spaced 3×5 Tx and Rx Vivaldi arrays is approximately 22 dB. In contrast, the proposed Tx beamforming approach achieves over 45 dB of isolation while maintaining high Tx array gain. Combined with the optimized Rx beamformer, the joint Tx-Rx approach provides more than 80 dB of overall IBFD system isolation, with minimal Rx gain loss—demonstrating both the effectiveness and practicality of the method.

Altogether, this work demonstrates that joint Tx-Rx beamforming is a powerful approach to overcoming the core SI challenge in IBFD systems. By directly addressing the scalability and performance trade-offs inherent in full-duplex operation, it brings us a significant step closer to realizing the full potential of next-generation, spectrally efficient wireless communication.

Keywords: In-Band Full-Duplex, Wireless Systems, Joint Transmit-Receive Beamforming, Self-Interference Mitigation, Receive Element/Array Isolation, System Isolation, Vivaldi Antenna Arrays, RFSoC.

List of Publications

This thesis is based on the following publications:

[A] **Mustafa Ayebe**, Johan Malmström, Sten E. Gunnarson, Henrik Holter, Marianna Ivashina, Carlo Bencivenni, Rob Maaskant, "Systematic Self-Interference Mitigation In Full Duplex Antenna Arrays Via Transmit Beamforming". *2023 International Conference on Electromagnetics in Advanced Applications (ICEAA), Venice, Italy, 2023.*

[B] **Mustafa Ayebe**, Rob Maaskant, Johan Malmström, Sten E. Gunnarson, Henrik Holter, Marianna Ivashina, "3D-printed Silver-coated Vivaldi Array With Integrated Coaxial Probe Feeding". *2024 IEEE International Symposium on Antennas and Propagation and INC/USNC-URSI Radio Science Meeting (AP-S/INC-USNC-URSI), Firenze, Italy, 2024.*

[C] **Mustafa Ayebe**, Rob Maaskant, Johan Malmström, Sten E. Gunnarson, Henrik Holter, Marianna Ivashina, "Evaluation of the Self-Interference Cancellation Limits of Full-Duplex Antenna Arrays Using Zynq UltraScale+ RF System-On-Chip Board". *2024 IEEE International Symposium on Phased Array Systems and Technology (ARRAY), Boston, MA, USA, 2024.*

[D] **Mustafa Ayebe**, Rob Maaskant, Johan Malmström, Sten E. Gunnarson, Marianna Ivashina, Henrik Holter, "Joint Tx-Rx Beamforming for Optimal Gain and Self-Interference Mitigation in In-Band Full-Duplex Arrays: Theory, Figures of Merit, and Validation". *IEEE Antennas and Wireless Propagation Letters (2025).*

[E] **Mustafa Ayebe**, Rob Maaskant, Marianna Ivashina, Johan Malmström, Sten E. Gunnarson, Henrik Holter, Simon Westergren, Erik Johansson , "In-Band Full-Duplex Antenna Beamforming and Synchronization for Self-Interference Mitigation: Multi-Tile RF-SoC Testbed Design and Deployment". *2025 19th European Conference on Antennas and Propagation (EuCAP), Stockholm, Sweden, 2025.*

Other publications by the author, not included in this thesis, are:

[F] **Mustafa Ayebe**, Rob Maaskant, "Electronic Device And Method In A Radio Network". *Patent no: WO2024170276A1, Aug, 2024.*

Acknowledgments

First and foremost, I would like to sincerely thank my supervisor, Prof. Rob Maaskant, for his continuous support and guidance throughout the years. His constructive feedback and creative ideas have been a great help during my research. I am also very grateful to Prof. Marianna Ivashina for her valuable academic suggestions and encouragement.

I would like to extend my thanks to every member of the Antenna Systems Group for providing a friendly and productive work environment. Special thanks to Teanette van der Spuy, Ashraf Uz Zaman, Oleg Lupikov, Pavlo Krasov, Usman Shehryar, Fitim Maxharraj, and Charitha Madapathage Don for their support–both in my research and personal life.

Furthermore, I am thankful to Henrik Holter, Sten Gunnarson, Johan Malmström, and everyone involved in the DIGIARRAY project, which is part of the Advanced Digitalization program at the WiTECH Centre. I appreciate the support and funding provided by VINNOVA, Ericsson, Saab, Satcube, and Chalmers.

Finally, and most importantly, I extend my deepest gratitude to my family for their selfless support, patience, and unconditional love. Without them, none of this would have been possible.

Acronyms

IBFD:	In-Band Full-Duplex
SIC:	Self-Interference Cancellation
MIMO:	Multiple Input Multiple Output
IoT:	Internet of Things
5G:	Fifth-Generation of cellular network technology
PA:	Power Amplifier
LNA:	Low Noise Amplifier
Tx:	Transmit
Rx:	Receive
$\mathbf{S}^{\mathrm{Rx,Tx}}$:	Tx-to-Rx Coupling Matrix
$\mathrm{ISO}^{\mathrm{Tx,Rx}}$:	Receiver Array Isolation
$\mathrm{ISO}_{m}^{\mathrm{Tx,Rx}}$:	Isolation of Receiver Element, m
$\mathrm{ISO}^{\mathrm{sys}}$:	In-Band Full-Duplex System Isolation
$\kappa^{\mathrm{Tx,Rx}}$:	The ratio of available Tx power to the LNA's 1 dB compression point
SSIR:	Signal to Self-Interference Ratio
maxGain:	Conventional Maximum Gain Beamformer
MRC:	Maximal Ratio Combining
MoM:	Method of Moment
RF:	Radio Frequency
RFSoC:	Radio Frequency System on Chip
ADC:	Analog to Digital Converter
DAC:	Digital to Analog Converter
EEP:	Embedded Element Pattern
dB:	Decibel
MTS:	Multi Tile Synchronization
PLL:	Phase Locked Loop
PL:	Programmable Logic
PS:	Processing System

Contents

Part I

Overview

CHAPTER 1

Introduction

This chapter provides an overview of in-band full-duplex (IBFD) communication, emphasizing its potential to double spectral efficiency by enabling simultaneous transmission and reception on the same frequency band. It introduces the primary challenge of self-interference (SI) and surveys existing SI mitigation techniques across different domains. The limitations of conventional methods motivate the exploration of joint transmit-receive (Tx-Rx) beamforming as a more effective solution. Furthermore, the chapter highlights key IBFD applications and outlines the research objectives and contributions, setting the stage for the theoretical developments and experimental validations presented in subsequent chapters.

1.1 Background on Full-Duplex Communication

Traditionally, wireless communication systems have operated in a half-duplex mode, utilizing either time-division duplexing or frequency-division duplexing to separate transmission and reception in time or frequency, respectively. While these methods effectively mitigate SI between transmitted and received signals, they result in suboptimal spectral efficiency, as only one communication direction is active at a given time or within a given frequency band [1].

In contrast, IBFD communication enables simultaneous transmission and reception over the same frequency band, theoretically doubling spectral efficiency and significantly enhancing system performance. As wireless networks face escalating demands for higher data rates, reduced latency, and more efficient spectrum usage, IBFD is increasingly recognized as a transformative technology [2], [3].

IBFD: Opportunities and Challenges

While IBFD has been standard in wired communication systems—such as traditional telephone networks, where separate physical channels prevent SI [4]—its realization in wireless systems has historically been hindered by the dominance of SI. In wireless settings, the transmitted signal often leaks into the receiver with power levels far exceeding that of the desired incoming signal, complicating reliable reception. However, recent advancements

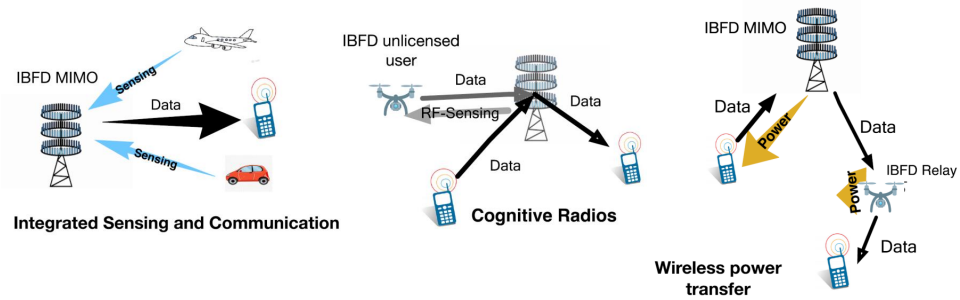

Figure 1.1: Emerging multifunctional transceivers are designed to support advanced services beyond conventional communications. Left: Integrated Sensing and Communication (ISAC) systems leverage full-duplex operation to concurrently perform wireless communication and environmental sensing. Center: Cognitive radio architectures use IBFD to perform real-time spectrum awareness while transmitting, enabling interference-aware spectrum access. Right: Wireless power transfer systems capable of simultaneously transferring energy and exchanging data, supporting efficient operation in power-limited scenarios (adapted from [6]).

in antenna design, signal processing, and RF hardware architectures have mitigated these challenges, positioning IBFD as a viable solution for next-generation wireless systems [5]. With spectrum resources becoming increasingly scarce, the ability of IBFD to dramatically improve frequency utilization makes it a critical enabler for future network evolution.

Key Applications

IBFD technology is a cornerstone of next-generation wireless transceivers that combine communication with other critical functions. As illustrated in Fig. 1.1, these multifunctional systems capitalize on the ability to transmit and receive simultaneously, enabling more efficient and adaptive wireless services.

The versatility of IBFD is being harnessed in several key application domains:

- **5G and Beyond**: Enables simultaneous uplink and downlink in massive multiple input multiple output (MIMO) deployments, enhancing spectral efficiency and leveraging beamforming for SI mitigation [7].
- **Cognitive Radio**: Supports real-time spectrum sensing during ongoing transmissions, allowing dynamic access to underutilized bands and improving spectrum utilization [2].
- **ISAC**: Facilitates the integration of sensing and communication, essential for applications like autonomous driving and smart infrastructure, where environmental awareness and data exchange are needed simultaneously [8].
- **Internet of Things (IoT) and Edge Computing**: Compact, energy-efficient IBFD transceivers support dense IoT networks, enhancing communication responsiveness and reducing latency in edge environments [9].
- **Satellite Communications**: Optimizes bandwidth usage in space-constrained non-terrestrial networks, such as LEO and GEO satellites, where full-duplex links address

propagation delays and spectrum limitations [10].

Self-Interference Cancellation

The primary technical barrier to practical IBFD implementation is effective self-interference cancellation (SIC) without degrading system performance. In wireless IBFD systems, SI arises from direct coupling between the Tx and Rx antennas, as well as from environmental reflections. These effects introduce both linear (e.g., direct leakage) and nonlinear (e.g., power amplifier distortion) interference components [11].

A typical IBFD receiver may experience SI signals up to 100 dB stronger than the desired received signal, necessitating exceptionally high suppression levels to prevent saturation and allow reliable signal detection [12]. The key challenges in achieving sufficient SI suppression include:

- **Dynamic SI Variability**: Environmental factors such as object motion, multipath fading, and temperature variations continuously alter SI characteristics, requiring adaptive cancellation mechanisms that can respond in real-time [5].

- **Compact Device Constraints**: In mobile and IoT devices where antenna separation is limited, maintaining sufficient isolation is more difficult, requiring innovative antenna design and SI mitigation strategies [13].

- **Trade-offs Across Cancellation Domains**: SI mitigation typically spans multiple domains—propagation, analog, and digital—each with inherent trade-offs. While analog cancellation (pre-ADC) prevents receiver front-end saturation, it is often power-hungry and scales poorly with large arrays. Digital cancellation (post-ADC) offers flexibility but demands precise modeling of nonlinearities and can introduce additional latency [14].

By addressing these challenges, IBFD technology promises to redefine the landscape of wireless communications, enhancing spectral efficiency and enabling advanced, high-performance wireless network architectures.

1.2 Existing Full-Duplex Mitigation Techniques

Figure 1.2 presents a representative architecture of an IBFD transceiver, along with the key components across different operational domains that will be discussed in the following sections. In the propagation domain, spatially separated multi-antenna arrays are employed for the Tx and Rx antenna arrays. Despite this physical separation, substantial SI remains due to direct coupling between antennas and environmental reflections from nearby scatterers, leading to dynamic and time-varying interference paths.

The analog domain encompasses the RF and analog circuitry between the antenna interfaces and the digital conversion stages. On the transmit side, the signal chain includes a multi-channel Digital-to-Analog Converter (DAC), frequency upconversion via a mixer, a Power Amplifier (PA), and the Tx antenna. The receive path follows a complementary structure: the Rx antenna feeds into a Low-Noise Amplifier (LNA), followed by frequency downconversion, multi-channel processing, and an Analog-to-Digital Converter (ADC). As shown in Figure 1.2, a cancellation circuit is integrated between the Tx and Rx paths. This canceller operates at the propagation frequency and is placed after the PA. In alternative

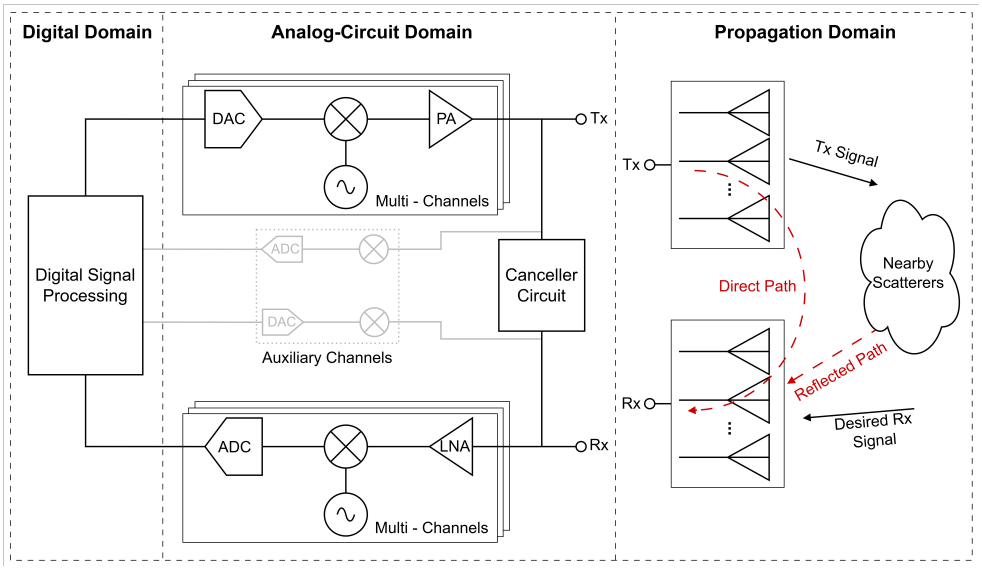

Figure 1.2: IBFD transceiver architecture, highlighting the propagation, analog-circuit, and digital domains.

architectures, auxiliary channels are used to facilitate SIC in both the analog and digital domains.

Lastly, the digital domain comprises a digital signal processing unit that manages all digital SIC procedures. The transceiver architecture illustrated in Figure 1.2 highlights the increasing complexity and integration of modern IBFD systems, where coordinated mitigation strategies span across the propagation, analog, and digital domains [15].

Propagation Domain

Propagation-domain techniques aim to minimize direct-path coupling between transmit and receive antennas. These methods can be broadly classified into passive and active categories.

Passive techniques use fixed configurations that do not require real-time adaptation, making them ideal for static environments with relatively stable interference characteristics:

- *Separation:* Physical distance and spatial orientation between antennas increase path loss or reduce radiation pattern overlap to attenuate interference [16].
- *Cross-Polarization:* Transmit and receive antennas operate on orthogonal polarizations (e.g., vertical and horizontal) to naturally minimize cross-coupling [17].
- *Surface Treatments:* Absorbers, reflective structures, and high-impedance surfaces, such as metasurfaces, are deployed around antennas to suppress surface currents and unwanted coupling [13], [18].
- *Coupling Networks:* Fixed impedance networks (resistors, capacitors, or inductors) inserted between antennas modify electromagnetic paths to reduce coupling [19].
- *Phase Control:* Antenna configurations introduce fixed phase shifts to create near-field nulls at the receiver. Examples include antiphase setups (180° phase shift) and

circular-mode techniques using Butler matrices for omnidirectional coverage [20].

Active techniques employ real-time tunable elements to adaptively suppress interference, better suiting dynamic environments:

- *Transmit Beamforming:* By adjusting the amplitude and phase of multiple Tx antennas, the near-field radiation pattern of a Tx array can be shaped to create a null at the receive antenna port, thereby reducing SI [21], [22].
- *Tunable Coupling Networks:* Variable-impedance components, such as varactors, are actively tuned to counter changing environmental conditions and minimize coupling [23].

While propagation-domain methods effectively target direct paths, they remain vulnerable to environmental reflections and time-varying channels, necessitating complementary circuit and digital approaches.

Analog-Circuit Domain

Analog-circuit domain techniques mitigate SI by subtracting an interference replica before the ADC stage, preventing receiver saturation. Adaptive analog cancellers typically achieve 50–60 dB suppression [24], [25].

Analog cancellation approaches are categorized into:

- *Channel-unaware methods:* Passive suppression circuits primarily address direct-path SI [13], [16], [26].
- *Channel-aware active methods:* Adaptive circuits dynamically adjust to both direct and reflected interference paths [25].

For narrowband applications, SI channels can be approximated using simple delay and gain models [13], [25]. Wideband signals, however, require more complex handling, often involving digital-domain assistance [27]. Effective analog cancellation depends heavily on accurate channel estimation and hardware calibration, with imperfections limiting suppression depth [25].

Architectural innovations include:

- *Frequency-domain cancellers:* Implement tunable bandpass filters, simplifying radio frequency (RF) integration and enabling cancellation before the LNA [4].
- *Time-domain cancellers:* Use tapped delay lines with variable amplitude and phase to recreate and subtract SI paths at RF or intermediate frequency [28], [29].
- *Digitally assisted cancellers:* Introduce auxiliary transmit paths whose digital control enables fine-grained cancellation [30].

Although analog cancellation provides essential early-stage suppression, it adds hardware complexity and is less effective against reflected and nonlinear components, making digital cancellation necessary for further mitigation.

Digital Domain

Digital-domain techniques address residual self-interference after ADC conversion. Their strength lies in flexibility, modeling and canceling diverse SI components via adaptive signal processing.

Typical digital cancellation strategies include:

- *Linear channel modeling:* Finite Impulse Response filters adaptively estimate and subtract SI [31].
- *Widely linear models:* Address IQ imbalance by modeling both interference and image signals [32].
- *Reference-based cancellation:* Use an auxiliary receiver to capture the actual transmitted signal—including distortions and noise—improving cancellation precision [33].
- *Nonlinear modeling:* Techniques such as memory polynomials compensate for PA-induced nonlinear SI, becoming critical at higher transmit powers [34].
- *Receive beamforming:* With sufficient antenna resources, digital beamforming techniques suppress SI spatially while preserving desired signals [35].

While digital SIC methods offer fine-grained adaptability, they rely on sufficient suppression in the analog and propagation domains to be effective. Their performance is fundamentally constrained by the dynamic range of the ADC; without adequate early-stage suppression, strong SI can overwhelm the ADC, making it impossible to recover the desired signal [36].

Hybrid Approaches

Recognizing the limitations of individual techniques, hybrid strategies integrate suppression across all domains—propagation, analog-circuit, and digital—to meet the stringent SI cancellation requirements of IBFD systems. A typical hybrid system might allocate:

- ~ 20 dB from antenna isolation,
- ~ 40 dB from analog cancellation,
- and the remaining suppression digitally,

achieving overall SI suppression exceeding 100 dB [26], [27]. Experimental validations show that combining propagation and analog approaches yields strong performance [16], and full system integrations have demonstrated up to 110 dB cancellation, enabling practical WiFi IBFD deployments [27]. Nevertheless, maintaining performance under dynamic conditions, such as mobile channels and rapidly changing environments, remains challenging.

Hybrid solutions often rely on sophisticated channel-aware techniques, including adaptive beamforming, but at the cost of increased hardware and computational complexity.

Beamforming-Based Approaches

Beamforming-based approaches leverage spatial signal processing to mitigate SI in IBFD systems, particularly in MIMO configurations. These methods can complement propagation, analog, and digital domain techniques by exploiting antenna array geometries to suppress SI through precoding and null-space projection, offering a powerful tool for achieving the high isolation required for simultaneous transmission and reception.

In a full-duplex MIMO system with N Tx and M Rx antennas, the SI channel is represented by an $N \times M$ matrix, $\mathbf{S}^{\mathrm{Rx,Tx}}$. Beamforming techniques aim to design a precoding matrix such that the transmitted signal falls into the null space of $\mathbf{S}^{\mathrm{Rx,Tx}}$, effectively nullifying SI at the receiver. When $N > M$, the SI channel matrix has at least $N - M$ zero

Table 1.1: Performance evaluation of measured IBFD systems using adaptive beamforming methods.

Ref	# of Tx, Rx elements	Beamforming method	Additional SIC scheme	f_c (GHz)	EIRP (dBm)	Total SIC (dB)
[21]	2, 1	Hybrid Tx	None	3.3	3.0	62.0
[22]	2, 1	Digital Tx	None	3	0.0^{+}	63.0
[39]	4, 4	Digital Tx and Rx	Digital	2.45	44.8	140.5
[40]	8, 1	Hybrid Tx	Prop. & Analog	2.45	22.7	96.0
[41]	4, 4	Digital Tx	Digital	2.4	10.0	76.0
[42]	2, 4	Digital Tx and Rx	None	4.5	12.0	97.0
[43]	36, 36	Digital Tx	Digital	2.4	0.0^{+}	87.0
[44]	8, 8*	Analog Tx and Rx	Prop. & Digital	0.73	16.5	100.0

$^{+}$ Antenna array gain was not reported, so it was not included in the EIRP calculation.
* Circulators enabled the sharing of antenna elements for both transmission and reception.

eigenvalues with corresponding eigenvectors, providing degrees of freedom for null-space projection [37].

To enhance full-duplex data rates, iterative beamforming strategies have been proposed for phased array systems [38]. This approach optimizes the Tx and Rx beamformer weights to achieve wideband SI cancellation purely in the spatial domain. It reduces the need for specialized RF cancellation circuitry while preserving both Tx and Rx gain.

Table 1.1 summarizes the performance of measured IBFD systems employing adaptive beamforming techniques. The table highlights key parameters, including the number of Tx and Rx antennas, beamforming methods, additional cancellation techniques, Effective Isotropic Radiated Power (EIRP), and total SI suppression achieved. Beamforming alone can provide at least 62 dB of SI cancellation, as seen in [21], [22]. However, many systems combine beamforming with propagation, analog, and digital cancellation methods to achieve higher suppression levels, up to 140.5 dB in advanced configurations [39]. These hybrid implementations underscore the synergy between beamforming and the techniques discussed in the previous subsections, where propagation-domain, analog cancellation, and digital signal processing collectively address diverse SI components.

Despite their effectiveness, beamforming-based approaches face several challenges that limit their practical deployment:

- *Channel Knowledge and Precision:* Null-space projection assumes perfect knowledge of the SI channel matrix, $\mathbf{S}^{\mathrm{Rx,Tx}}$, and infinite precision in digital signal processing. In practice, channel estimation errors and finite precision lead to residual SI, requiring a trade-off between SI suppression and beamforming performance. For effective nulling, the number of Tx antennas (N) must exceed the number of Rx antennas (M), but a large disparity degrades Rx beamforming quality, reducing communication performance.

- *Latency in Iterative Methods:* Joint Tx and Rx beamforming, often implemented through iterative optimization, can be computationally intensive and slow, increasing system latency in dynamic environments where real-time adaptation is critical.

- *Nonlinear Constraints:* Beamforming strategies typically do not account for the maximum input power limits of LNAs to prevent nonlinear gain compression. Relying solely on nulling SI at the receiver inputs imposes stringent constraints, often necessitating larger Tx antenna arrays or additional hardware cancellation circuits, which increase complexity and cost.

- *Reliance on Complementary SIC Methods:* Table 1.1 shows that beamforming alone is often insufficient for effective self-interference suppression, with many systems requiring additional SIC techniques to achieve the desired performance.

Despite considerable progress, a persistent trade-off exists between achieving high suppression, maintaining system gain, and limiting implementation overhead. This challenge motivates the exploration of innovative frameworks.

1.3 Proposed Joint Tx-Rx Beamforming

The research, as presented in this thesis, introduces a novel joint Tx-Rx beamforming approach tailored for IBFD antenna arrays [45]. Unlike traditional methods, the proposed technique simultaneously optimizes transmission and reception to fulfill two critical objectives:

- **Maximize Tx array gain while constraining SI at the Rx input**: The method ensures that the self-interference at the LNA input remains below a predetermined limit, typically set relative to the LNA's 1 dB compression point with appropriate modulation backoff. This constraint preserves the linearity of the receiver chain, maintaining signal integrity and preventing receiver saturation.
- **Suppress residual SI at the receiver output**: Beyond initial mitigation at the antenna interface, the approach further reduces SI post-LNA, enhancing the signal-to-SI ratio (SSIR) and improving the receiver's ability to recover the desired signal even in challenging environments.

By jointly considering the Tx and Rx paths during beamforming optimization, the proposed method achieves a more favorable trade-off between SI suppression and system performance than conventional designs, laying the groundwork for more robust and efficient IBFD systems.

1.4 Research Objectives and Contributions

Building upon the concept of joint Tx-Rx beamforming, this research aims to advance IBFD technology through a rigorous theoretical and experimental investigation. The specific objectives are:

- **Develop a comprehensive theoretical framework**: A systematic formulation for joint Tx-Rx beamforming is proposed, capturing the essential trade-offs between maximizing Tx gain and minimizing SI at the receiver. The framework accommodates practical constraints, such as hardware limitations and SI power thresholds.
- **Define novel performance metrics**: Recognizing that traditional metrics like array gain and SI suppression do not fully capture IBFD system behavior, new figures of merit are introduced to evaluate the overall effectiveness of the joint optimization strategy.
- **Experimentally validate the proposed approach**: A practical testbed is developed based on a Radio Frequency system on chip (RFSoC) evaluation board integrated with custom 3×5 element Vivaldi antenna arrays for both transmission and reception. Experimental results demonstrate the feasibility and advantages of the joint Tx-Rx beamforming method under realistic conditions.

The key contributions of this work lie in offering a practical, scalable, and effective SI mitigation strategy for IBFD systems. By addressing the core challenges of IBFD systems, this research paves the way for their deployment in next-generation wireless networks, where efficient spectrum utilization and high data rates are increasingly critical.

1.5 Outline of the Thesis

The remainder of this thesis is organized as follows:

- **Chapter 2** introduces the proposed system framework for a non-shared aperture IBFD antenna array and develops an optimal joint Tx-Rx beamforming strategy. It presents the underlying system modeling, defines key performance metrics including array and system-level isolation, and formulates the beamforming optimization problems for both the Tx and Rx chains. The effectiveness of the proposed approach is demonstrated through detailed numerical simulations, highlighting its ability to suppress SI while maintaining high antenna performance.

- **Chapter 3** presents the practical implementation, measurement setup, and experimental validation of the proposed joint Tx/Rx beamforming method for IBFD systems. A full-duplex testbed is developed using integrated Vivaldi antenna arrays and a programmable RFSoC platform. The experimental results are compared with simulations to evaluate system performance, focusing on antenna gain, SI suppression, and overall beamforming robustness under realistic hardware impairments.

- **Chapter 4** concludes the thesis by summarizing the main findings, highlighting key contributions, and proposing directions for future research to advance practical IBFD systems.

CHAPTER 2

IBFD Antenna Array System Framework and Optimal Beamforming

2.1 Non-Shared Aperture IBFD System Framework

A dual-aperture IBFD system model is considered, comprising an N-element Tx antenna array and an M-element Rx antenna array, as depicted in Figure 2.1. Each antenna element is individually connected to its dedicated PA on the Tx side and LNA on the Rx side, with associated beamforming networks controlling the signal paths.

The system behavior is described using scattering (S) parameters and power waves, following the formalism introduced in [46]. In this framework, the a-waves represent the incident power waves entering the front-end ports, while the b-waves represent the outgoing power waves.

Referring to Figure 2.1, the Tx beamforming vector $\mathbf{w}^{\mathrm{Tx}}$ defines the amplitude and phase excitation across the transmit elements. These excitations are subsequently amplified by the PAs, resulting in the power wave vector $\mathbf{a}^{\mathrm{Tx}}$ at the Tx input ports. On the receiver side, the conjugated Rx beamforming vector, $(\mathbf{w}^{\mathrm{Rx}})^*$, controls the weighting applied to the received signals. After amplification by the LNAs, the outgoing waves at the Rx ports are represented by the vector $\mathbf{b}^{\mathrm{Rx}}$. The interactions between the incident and outgoing waves at the system's front-end are modeled by the following matrix equation:

$$\begin{bmatrix} \mathbf{b}^{\mathrm{Tx}} \\ \mathbf{b}^{\mathrm{Rx}} \end{bmatrix} = \begin{bmatrix} \mathbf{S}^{\mathrm{Tx,Tx}} & \mathbf{S}^{\mathrm{Tx,Rx}} \\ \mathbf{S}^{\mathrm{Rx,Tx}} & \mathbf{S}^{\mathrm{Rx,Rx}} \end{bmatrix} \begin{bmatrix} \mathbf{a}^{\mathrm{Tx}} \\ \mathbf{a}^{\mathrm{Rx}} \end{bmatrix} + \begin{bmatrix} \mathbf{0} \\ \mathbf{b}^{\mathrm{Rx}}_{\mathrm{sig}} \end{bmatrix} \tag{2.1}$$

where $\mathbf{S}$ is the overall system scattering matrix that captures the transmission, reflection, and coupling characteristics between the Tx and Rx ports.

To simplify the analysis, we assume that the reflections at the LNA inputs are negligible, i.e., $\mathbf{a}^{\mathrm{Rx}} = \mathbf{0}$. This assumption is reasonable because integrated beamformer chips are typically low-power, and any small reflection signals $\mathbf{a}^{\mathrm{Rx}}$ have a negligible impact on the overall system performance. Under this assumption, the outgoing Rx power waves, $\mathbf{b}^{\mathrm{Rx}}$, comprise two components:

- $\mathbf{b}^{\mathrm{Rx}}_{\mathrm{sig}}$, which represents the desired signal waves resulting from an external incident electromagnetic field, $\mathbf{E}_{\mathrm{inc}}$;

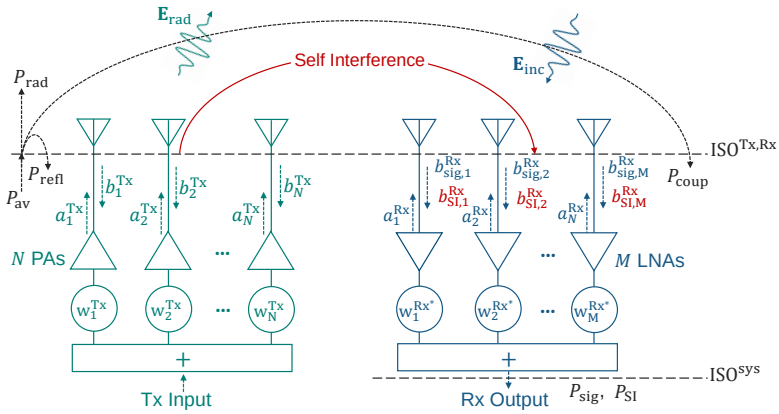

Figure 2.1: The considered non-shared aperture IBFD system architecture consists of an N-element Tx antenna array, with each element independently driven by a dedicated PA, and an M-element Rx antenna array, with each element interfaced to a dedicated LNA. Advanced beamforming networks are integrated at both the Tx and Rx arrays to precisely steer the radiated ($\mathbf{E}_{\text{rad}}$) and received ($\mathbf{E}_{\text{inc}}$) fields, thereby enabling highly directional transmission and reception while suppressing self interference.

- $\mathbf{b}_{\text{SI}}^{\text{Rx}}$, which corresponds to the SI waves due to the coupling between the Tx and Rx chains inherent in IBFD operation.

For the dual-aperture IBFD architecture, we define several important power metrics at the antenna front-end ports: the available power at the Tx ports P_{av}, the radiated power P_{rad}, and the coupled power received at the Rx ports P_{coup}. These quantities are mathematically expressed as:

$$\begin{aligned} P_{\text{av}}\left(\mathbf{w}^{\text{Tx}}\right) &= \frac{1}{2}\left(\mathbf{a}^{\text{Tx}}\right)^{\text{H}}\mathbf{a}^{\text{Tx}}, \\ P_{\text{rad}}\left(\mathbf{w}^{\text{Tx}}\right) &= \frac{1}{2\eta}\left(\mathbf{a}^{\text{Tx}}\right)^{\text{H}}\mathbf{G}^{\text{H}}\mathbf{G}\mathbf{a}^{\text{Tx}}, \\ P_{\text{coup}}\left(\mathbf{w}^{\text{Tx}}\right) &= \frac{1}{2}\left(\mathbf{b}_{\text{SI}}^{\text{Rx}}\right)^{\text{H}}\mathbf{b}_{\text{SI}}^{\text{Rx}} \quad \text{where} \quad \mathbf{b}_{\text{SI}}^{\text{Rx}} = \mathbf{S}^{\text{Rx,Tx}}\mathbf{a}^{\text{Tx}}, \end{aligned} \tag{2.2}$$

where $(\cdot)^{\text{H}}$ denotes the Hermitian (conjugate transpose) operator, η is the characteristic impedance of free space, and $\mathbf{G}$ is the column-augmented matrix composed of the embedded element patterns (EEPs) of the Tx antenna array, i.e., $\mathbf{G} = [\boldsymbol{G}_1, \boldsymbol{G}_2, \ldots, \boldsymbol{G}_N]$. Each $\boldsymbol{G}_n$ represents the complex far-field EEP for the n-th Tx element, corresponding to the case when element n is excited with a unit amplitude incident wave while all other elements are properly terminated [47].

It is important to note that the coupled power P_{coup} depends solely on the Tx beamforming vector $\mathbf{w}^{\text{Tx}}$ and is independent of the Rx beamformer. Consequently, the design of the Tx beamformer plays a critical role in minimizing the power leakage into the Rx chain and preventing saturation of the LNA front-ends. As illustrated in Figure 2.1, the SI arises through mutual coupling between the Tx and Rx array elements. With optimal choice of $\mathbf{w}^{\text{Tx}}$, it is theoretically possible to arrange the Tx element excitations such that the coupled powers destructively interfere, minimizing the total SI observed at the Rx ports. However, this SI suppression must be balanced against the requirement for efficient radiation

performance of the antenna array.

To characterize the effectiveness of the Tx beamforming strategy in suppressing coupled SI, we introduce the notion of **Rx array antenna isolation** in [45], defined as the ratio of the available transmit power to the coupled power at the receiver:

$$\mathrm{ISO}^{\mathrm{Tx,Rx}}(\mathbf{w}^{\mathrm{Tx}}) = \frac{P_{\mathrm{av}}(\mathbf{w}^{\mathrm{Tx}})}{P_{\mathrm{coup}}(\mathbf{w}^{\mathrm{Tx}})}. \tag{2.3}$$

Furthermore, when focusing on the m-th receiving element individually, the coupled power observed at that specific LNA input can be expressed as

$$P_{\mathrm{coup},m} = \frac{1}{2}\left(\mathbf{a}^{\mathrm{Tx}}\right)^{\mathrm{H}}\left(\boldsymbol{S}_m^{\mathrm{Rx,Tx}}\right)^{\mathrm{H}}\boldsymbol{S}_m^{\mathrm{Rx,Tx}}\mathbf{a}^{\mathrm{Tx}}, \tag{2.4}$$

where $\boldsymbol{S}_m^{\mathrm{Rx,Tx}}$ denotes the m-th row of the coupling matrix between the Tx and Rx arrays. In this case, the array isolation $\mathrm{ISO}^{\mathrm{Tx,Rx}}(\mathbf{w}^{\mathrm{Tx}})$ simplifies to the **Rx element isolation**, denoted $\mathrm{ISO}_m^{\mathrm{Tx,Rx}}$. It is important to highlight that the isolation observed at an individual Rx element typically exceeds the isolation achieved across the entire array. This is because the total coupled power P_{coup} aggregates the contributions from all Rx elements (a detailed proof can be found in [45]). This observation guides the practical design of IBFD systems: isolation requirements should slightly exceed the minimum achievable element isolation to ensure robust system performance while avoiding over-constraining the beamforming design.

However, even if the Tx beamformer successfully prevents saturation of the Rx front-end, the residual coupled power may still greatly exceed the power of the desired received signal. Consequently, it becomes essential to design an effective Rx beamformer to further suppress SI and to preserve the sensitivity and linearity of the receiver modem.

To quantify the impact of the receive beamforming, we define the total desired received signal power P_{sig} and the residual SI power P_{SI} at the output ports of the Rx beamformer as:

$$\begin{aligned} P_{\mathrm{sig}}\left(\mathbf{w}^{\mathrm{Rx}}\right) &= \frac{1}{2}\left|\left(\mathbf{w}^{\mathrm{Rx}}\right)^{\mathrm{H}} S_{21}^{\mathrm{LNA}}\mathbf{b}_{\mathrm{sig}}\right|^2, \\ P_{\mathrm{SI}}\left(\mathbf{w}^{\mathrm{Tx}},\mathbf{w}^{\mathrm{Rx}}\right) &= \frac{1}{2}\left|\left(\mathbf{w}^{\mathrm{Rx}}\right)^{\mathrm{H}} S_{21}^{\mathrm{LNA}}\mathbf{b}_{\mathrm{SI}}\right|^2, \end{aligned} \tag{2.5}$$

where S_{21}^{LNA} denotes the voltage gain of the LNAs. In this formulation, it is assumed that the system operates under an SI-dominated regime, thereby neglecting the contributions of thermal noise or other noise sources. This assumption is justified in typical IBFD scenarios, where the SI power often overwhelms the noise floor unless substantial suppression is achieved.

Finally, to assess the joint effectiveness of the Tx and Rx beamformers, we define the **total IBFD system isolation** in [45] at the Rx beamformer output port as:

$$\mathrm{ISO}^{\mathrm{sys}} = \frac{P_{\mathrm{av}}(\mathbf{w}^{\mathrm{Tx}})}{P_{\mathrm{SI}}(\mathbf{w}^{\mathrm{Tx}},\mathbf{w}^{\mathrm{Rx}})}. \tag{2.6}$$

This system-level isolation metric captures the combined impact of the transmit and receive beamforming strategies on mitigating SI and serves as a key performance indicator for the design and optimization of practical IBFD systems.

2.2 Optimal Joint Tx-Rx Beamforming Approach

We propose a joint Tx-Rx optimal beamforming framework [45] that leverages SIC capabilities on both ends of the link, while dynamically adapting to beam-steering requirements. On the transmit side, the beamformer is designed to maintain SI resulting from Tx-to-Rx coupling below a predefined threshold, thereby preventing receiver front-end saturation while simultaneously maximizing antenna gain. On the receive side, the beamformer modifies the conventional maximal ratio combining (MRC) approach to additionally suppress residual SI below a tolerable threshold, thus maintaining a high SSIR and effectively isolating the desired signal from the interference.

Tx Beamforming

The transmit beamforming strategy optimizes the excitation weights $\mathbf{w}^{\mathrm{Tx}}$ by incorporating prior knowledge of the Tx-to-Rx coupling matrix, $\mathbf{S}^{\mathrm{Rx,Tx}}$, estimated from a digital self-interference channel. While the optimization builds upon the structure of a *conventional Tx maximum gain beamformer* [48], it introduces a key modification: enforcing a minimum Rx array antenna isolation threshold, denoted by $\kappa^{\mathrm{Tx,Rx}}$. This threshold is defined as the ratio of the available transmit power P_{av} to the LNA's 1 dB compression point, factoring in backoff requirements due to signal modulation. Enforcing $\kappa^{\mathrm{Tx,Rx}}$ ensures the linear operation of the receiver chain by preventing saturation.

The Tx beamforming problem is formulated as follows [45], [49]:

$$\begin{aligned} \max_{\mathbf{w}^{\mathrm{Tx}}} \quad & \frac{P_{\mathrm{rad}}(\mathbf{w}^{\mathrm{Tx}})}{P_{\mathrm{av}}(\mathbf{w}^{\mathrm{Tx}})} \\ \text{subject to} \quad & \begin{cases} \mathrm{ISO}^{\mathrm{Tx,Rx}}(\mathbf{w}^{\mathrm{Tx}}) \geq \kappa^{\mathrm{Tx,Rx}}, \\ (\mathbf{w}^{\mathrm{Tx}})^{\mathrm{H}}\mathbf{w}^{\mathrm{Tx}} = 1. \end{cases} \end{aligned} \tag{2.7}$$

After obtaining the optimal transmit beamformer $\mathbf{w}^{\mathrm{Tx}}_{\mathrm{opt}}$, the resulting minimum element isolation, $\min(\mathrm{ISO}^{\mathrm{Tx,Rx}}_m)$, can be evaluated. If this minimum isolation significantly exceeds the required threshold for preventing saturation, the isolation constraint $\kappa^{\mathrm{Tx,Rx}}$ may be iteratively relaxed to ensure that $\min(\mathrm{ISO}^{\mathrm{Tx,Rx}}_m)$ remains just above the required level, optimizing both system performance and beamforming efficiency.

Rx Beamforming

On the receive side, the beamforming vector $(\mathbf{w}^{\mathrm{Rx}})^*$ is optimized to maximize the received desired signal power, following the conventional MRC criterion, while simultaneously ensuring that the residual SI power does not exceed a specified threshold κ_{SI}. This threshold is typically selected to match the receiver noise floor, thereby guaranteeing that the SI does not degrade receiver sensitivity.

The optimal Rx beamforming method is drawn out as follows [45]:

$$\begin{aligned} \max_{\mathbf{w}^{\mathrm{Rx}}} \quad & P_{\mathrm{sig}}(\mathbf{w}^{\mathrm{Rx}}) \\ \text{subject to} \quad & \begin{cases} P_{\mathrm{SI}}(\mathbf{w}^{\mathrm{Tx}}, \mathbf{w}^{\mathrm{Rx}}) \leq \kappa_{\mathrm{SI}}, \\ (\mathbf{w}^{\mathrm{Rx}})^{\mathrm{H}}\mathbf{w}^{\mathrm{Rx}} = 1. \end{cases} \end{aligned} \tag{2.8}$$

By jointly optimizing both the Tx and Rx beamformers according to the criteria outlined

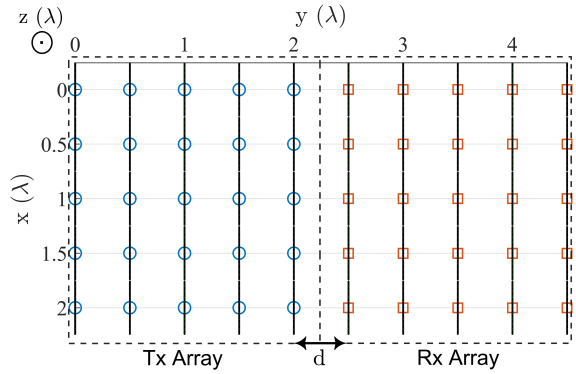

Figure 2.2: Dual-aperture IBFD antenna configuration: 5×5 Tx and Rx arrays of x-polarized dipole antennas, each 0.49λ long with 0.5λ spacing within each array. The operating wavelength $\lambda = \frac{c}{f_c}$, where c is the speed of light and f_c is the design frequency. The arrays are separated by $d = 0.5\lambda$, and both are elevated $\lambda/4$ above a perfect electrically conducting ground plane located in the xy-plane. The H- and E-planes are defined as the yz- and xz-planes, respectively.

above, the IBFD system achieves robust SI suppression while maintaining high-quality desired signal reception, enabling practical full-duplex wireless communication even in the presence of significant Tx-Rx coupling.

2.3 Proof of Concept: Performance Evaluation

To validate the proposed beamforming framework, a proof-of-concept simulation is conducted using 5×5 Tx and Rx arrays of x-polarized dipole antennas configured as shown in Figure 2.2. The electromagnetic simulation is performed using an in-house Method-of-Moments (MoM) code, CAESAR [50], and the beamforming algorithms are implemented and evaluated in MATLAB.

Tx Beamforming

The eigenvalue spectrum of $[(\mathbf{S}^{\mathrm{Rx,Tx}})^{\mathrm{H}}\mathbf{S}^{\mathrm{Rx,Tx}}]^{-1}$ shown in Figure 2.3(a) reveals the available degrees of freedom for constructing the Tx beamforming vector $\mathbf{w}^{\mathrm{Tx}}$ that satisfies an isolation constraint $\kappa^{\mathrm{Tx,Rx}}$. Only eigenvectors corresponding to eigenvalues above this threshold are utilized in beamforming. Figure 2.3(b) highlights the trade-off between maximizing the Tx realized antenna gain and enforcing increased isolation levels. As isolation constraints tighten, the realized Tx gain decreases—especially beyond $\pm 40^\circ$ scan angles—demonstrating the cost of aggressive SI suppression.

Figure 2.4 further illustrates that the proposed Tx beamformer, designed for isolation, produces broader beam patterns in the H-plane due to a reduced set of usable eigenmodes, while maintaining comparable performance in the E-plane. Additionally, while the Tx antenna gain pattern of the proposed beamformer degrades at large H-plane scan angles, its performance in the E-plane remains largely unaffected.

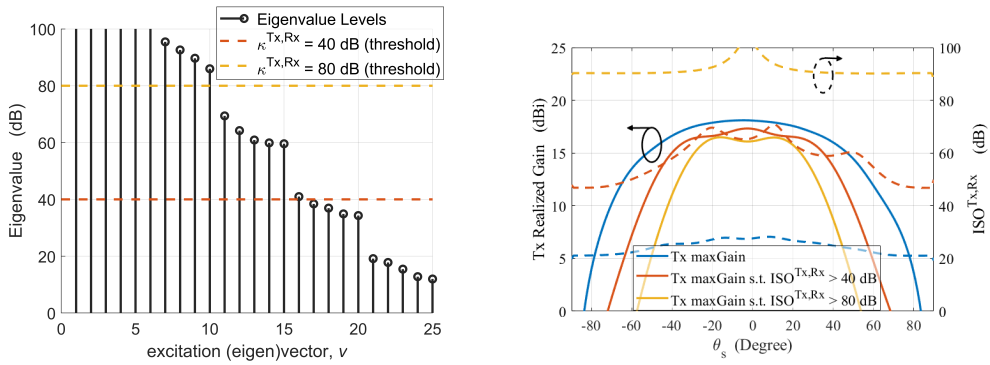

Figure 2.3: (a) Eigenvalue spectrum of $[(\mathbf{S}^{\mathrm{Rx,Tx}})^{\mathrm{H}}\mathbf{S}^{\mathrm{Rx,Tx}}]^{-1}$ for different $\kappa^{\mathrm{Tx,Rx}}$ values. (b) Trade-off between Tx realized array gain and Rx array isolation under varying isolation constraints over H-plane scan angles.

As seen in Figure 2.5(a), the element-level isolation consistently exceeds the overall array isolation by 10–20 dB depending on scan angle and element index. To prevent overdesign, isolation constraints can be relaxed iteratively until the minimum element isolation $\min(\mathrm{ISO}_m^{\mathrm{Tx,Rx}})$ just satisfies the linearity requirement, as illustrated in Figure 2.5(b).

Figure 2.6 illustrates the isolation bandwidth performance, demonstrating stable isolation over approximately 400 MHz when the Tx beamformer coefficients, $\mathbf{w}^{\mathrm{Tx}}$, are optimized at the center frequency f_c. In Figure 2.7, increasing antenna separation logarithmically expands the subspace of usable eigenvectors, enhancing beamforming flexibility.

Lastly, the process of connecting the beamforming circuitry introduces variations in the antenna loading conditions, which can affect the Rx array and element-level isolation between ports. To assess the impact of this effect, we examined the eigenvalue spectrum of the Tx–Rx coupling matrix under perturbed loading conditions. Specifically, the port impedances were equally varied within a range of $Z_0 \pm 0.2Z_0$ Ω to reflect potential mismatches introduced by practical beamformer chip implementations.

The resulting analysis revealed that the changes in Rx array-level isolation were less than 4 dB, while variations in Rx minimum element-level isolation remained below 3 dB. Given that these deviations are relatively small and do not significantly impact the system's overall isolation performance, plots of this analysis are not included in this thesis.

Rx Beamforming

Figure 2.8 compares the Rx realized array gain and IBFD system isolation between a conventional MRC beamformer and the proposed Rx beamformer constrained to $P_{\mathrm{SI}} = -80$ dBW when the Tx maxGain beamformer is applied to the Tx array. The proposed beamformer maintains comparable gain while significantly enhancing isolation.

Lastly, Figure 2.9 evaluates the IBFD system-level isolation bandwidth when the Rx weights are optimized at f_c when the Tx antenna array is excited toward broadside with a maxGain beamformer. As frequency deviates from f_c, isolation degrades—indicating the need for frequency-adaptive beamforming to maintain IBFD performance over wider bands.

The results demonstrated clear trade-offs between isolation and gain, along with prac-

tical techniques to tune beamformer constraints to meet system linearity requirements. Performance was evaluated across beam scan angles, frequency, and antenna separations, confirming the robustness and flexibility of the proposed method. These findings establish a strong foundation for extending the framework to include frequency-aware beamforming or digital cancellation techniques in future research.

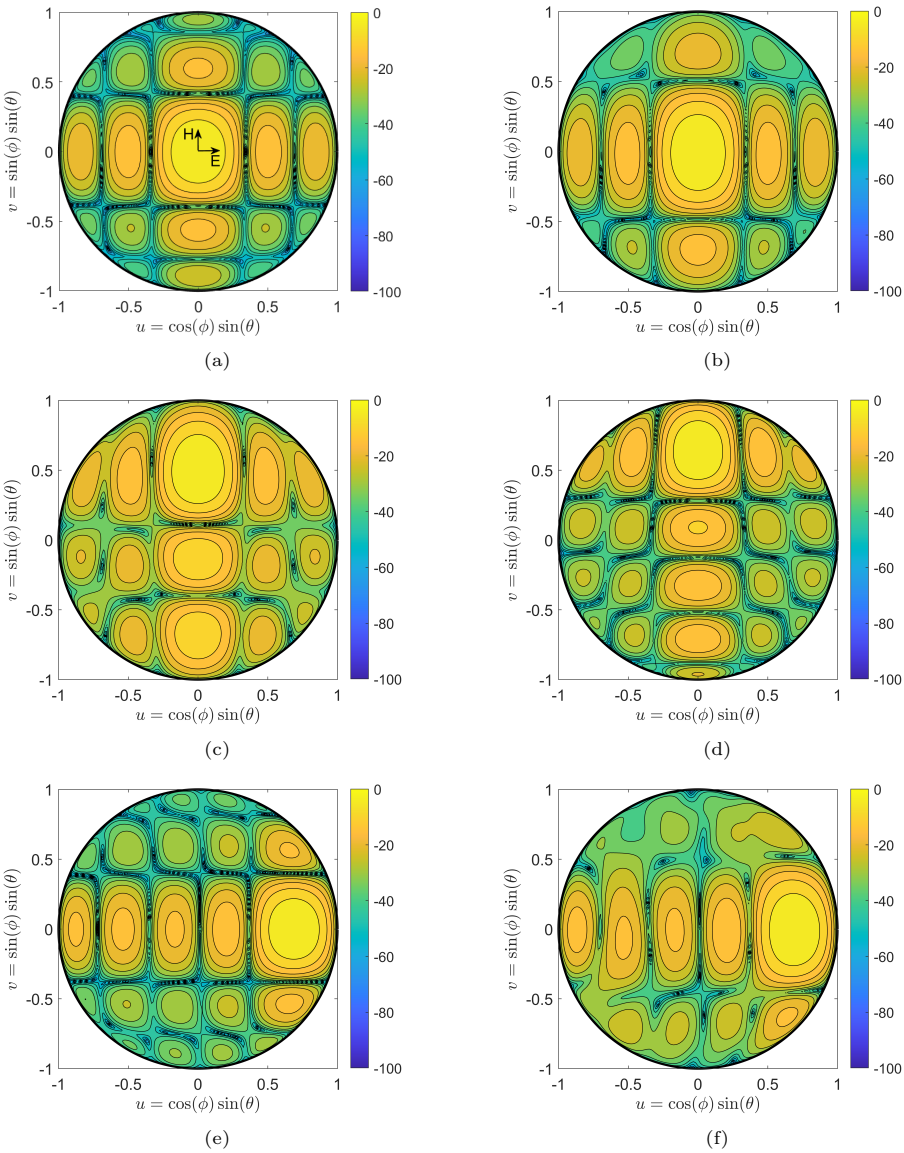

Figure 2.4: Normalized Tx antenna array patterns comparing conventional maxGain beamformer vs. proposed beamformer with $\mathrm{ISO}^{\mathrm{Tx,Rx}} > 40$ dB: (a)–(b) broadside H-plane; (c)–(d) 45° H-plane; (e)–(f) 45° E-plane.

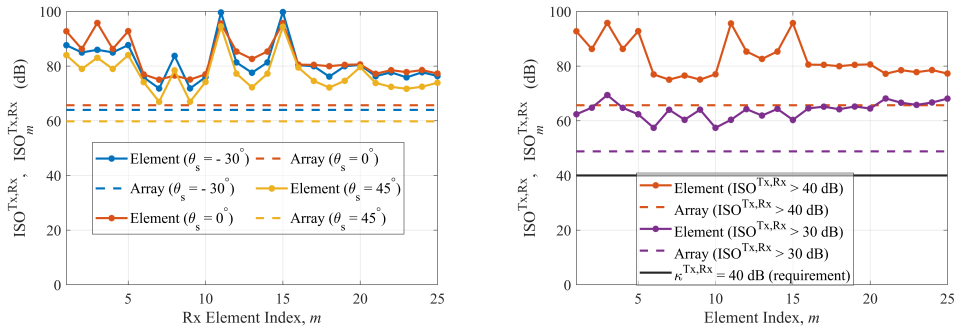

(a) (b)

Figure 2.5: (a) Rx array vs. element isolation for various H-plane scan angles with $\text{ISO}^{\text{Tx,Rx}} > 40$ dB. (b) Isolation tuning via iterative threshold relaxation for broadside scan.

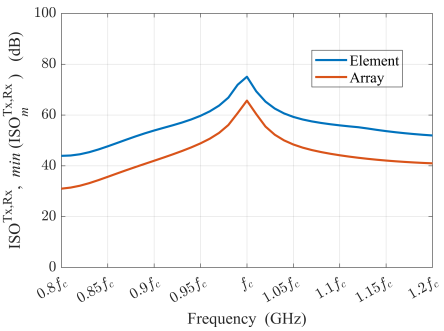

Figure 2.6: Minimum Rx element and array isolation across frequency for the proposed Tx beamformer s.t. $\text{ISO}^{\text{Tx,Rx}} > 40$ dB at broadside scan.

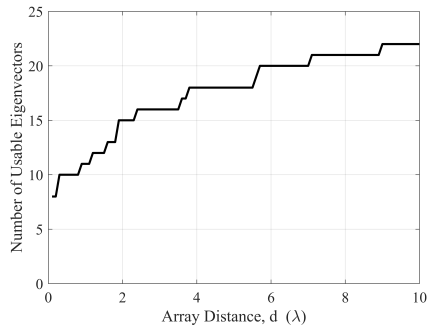

Figure 2.7: Usable eigenvectors vs. Tx–Rx array separation d for $\kappa^{\text{Tx,Rx}} = 80$ dB.

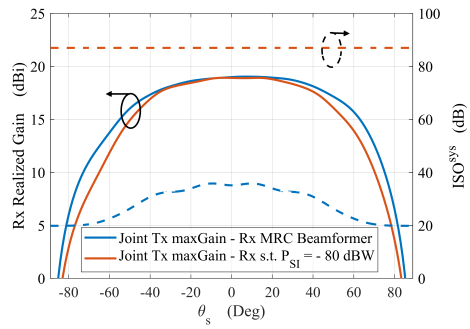

Figure 2.8: Rx realized array gain and system isolation over H-plane scan angles for MRC vs. proposed Rx beamformer ($P_{\text{SI}} = -80$ dBW) when Tx maxGain beamformer is applied.

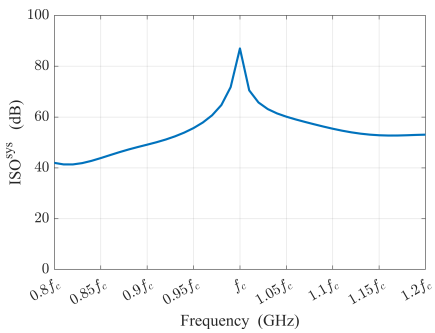

Figure 2.9: IBFD system isolation across frequency at broadside scan using proposed Rx beamformer.

CHAPTER 3

Integrated IBFD System: Testbed Design and Experimental Validation

3.1 IBFD Testbed and Case Study Setup

To validate the proposed beamforming framework, we developed a practical IBFD testbed system. Our selected case study, illustrated in Figure 3.1, features an IBFD system incorporating 3×5 element Tx and Rx Vivaldi antenna arrays, operating over the 3–6 GHz frequency range [51].

The Tx and Rx arrays are positioned side-by-side with maximum element and sub-array spacing constrained to 0.5λ at 6 GHz, resulting in strong mutual coupling between the arrays — a key aspect for evaluating SI mitigation performance. Each antenna array is interfaced with a custom-designed printed circuit board utilizing commercial off-the-shelf baluns[1], which convert unbalanced signals from the RF paths to differential interfaces suitable for DACs and ADCs. These boards interface directly with the Zynq UltraScale+ RFSoC ZCU216 evaluation platform for signal generation and processing.

Tx–Rx Antenna Array Design

Antenna Element Structure: Each antenna element is based on a Vivaldi design, realized from a single 3D-printed and subsequently metalized structure. The feed is implemented via a $50\,\Omega$ coaxial probe connected through the ground plane. To prevent grating lobes during beam steering up to 6 GHz, the element spacing is maintained at $\lambda/2$ at the highest operating frequency. Figure 3.2(a) shows the unit-cell model of the proposed Vivaldi element, highlighting the optimized parameters, including cavity size, slot geometry, Vivaldi taper length, and taper opening rate [52].

Manufacturing Process: A small-scale 1×5 array prototype was fabricated using a Halot Mage 8K Resin 3D printer, offering a fine $29.7\,\mu$m XY resolution and compatibility with light-reactive thermoset materials. Post-printing, the antenna structures were cleaned and subsequently coated with multiple layers of water-based EMI silver conductive paint (842WB) using a manual brush application. This process resulted in robust and electrically conductive antenna surfaces. Figure 3.2(b) presents the final silver-coated 1×5 Vivaldi

[1] Product No: X4BD40L1-50100G

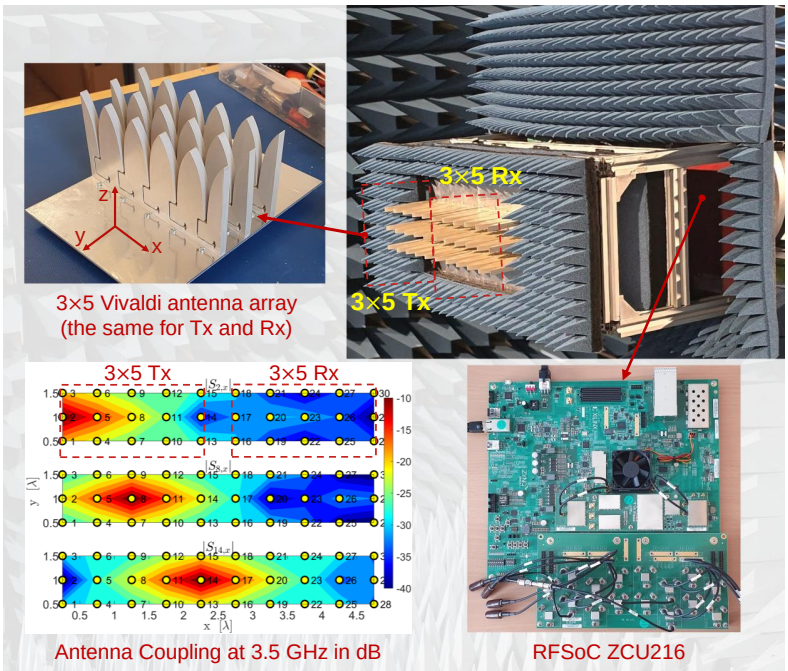

Figure 3.1: Case study: Experimental IBFD antenna system consisting of side-by-side 3×5 Tx and Rx Vivaldi arrays. The system is integrated with the Zynq UltraScale+ RFSoC ZCU216 evaluation kit and deployed inside an anechoic chamber for measurement and validation.

array with integrated coaxial probe feeds.

Simulation and Experimental Validation: Simulations of the infinite array model showed active reflection coefficients better than -10 dB for beam steering up to $\pm 60°$ in the E-plane and $\pm 50°$ in the H-plane across the 3–6 GHz band. Measurements on the fabricated 1×5 array prototype confirmed these simulation results, validating the embedded element design and coaxial feed structure, as detailed in [51].

Building upon this validated design, the Tx and Rx arrays were scaled up to full 3×5 element configurations. Each element is fed via an individually mounted coaxial probe on a shared aluminum ground plane, as shown in Figure 3.1.

The RFSoC ZCU216 Platform

The integration of advanced RFSoC platforms, such as the Zynq UltraScale+ RFSoC ZCU216 evaluation board, has significantly accelerated the practical realization of digital beamforming and SIC techniques. Leveraging the board's real-time signal processing capabilities and high degree of system integration, it becomes feasible to support sophisticated custom antenna designs and execute complex tasks such as system calibration, IBFD communication, and joint sensing operations [22], [53].

The ZCU216 board is equipped with 16×14-bit DACs and 16×14-bit ADCs, organized into four independent DAC tiles and four independent ADC tiles. It supports direct RF signal conversion from DC up to 6 GHz. The DACs offer sampling rates up to 10 GSPS,

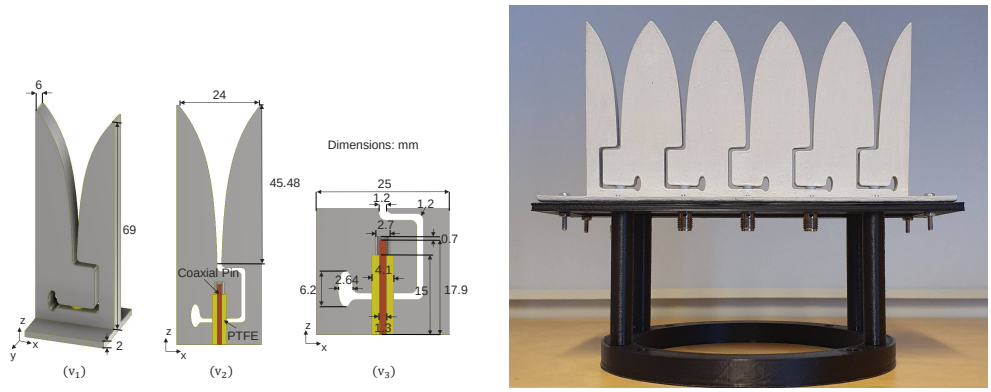

Figure 3.2: Vivaldi antenna array development: (a) Unit-cell geometry; (v_1) 3D view of the model, (v_2) Cross-section of the antenna element in the x-z plane, and (v_3) Detailed view of the feeding section, (b) Fabricated 1×5 Vivaldi array prototype after 3D printing and silver painting [51].

while the ADCs provide up to 2.5 GSPS, enabling wideband signal processing and direct RF interfacing without the need for additional up/down-conversion stages.

Precise synchronization between the transmit and receive paths is critical for achieving effective digital beamforming and reliable SIC performance. However, inherent phase shifts and clock drift introduced by the independent phase-locked loops (PLLs) associated with each DAC and ADC tile can cause significant misalignment. Such phase mismatches disrupt coherent operation, degrading the system's overall beamforming and cancellation performance.

To overcome this, the RFSoC architecture incorporates a multi-tile synchronization (MTS) feature. MTS utilizes a shared reference clock and a system reference (sysref) signal to synchronize the sample clocks across all DAC and ADC tiles [54]. Proper configuration ensures deterministic phase alignment and consistent timing across the entire RF interface.

Despite these built-in features, achieving robust MTS on the ZCU216 board with default Xilinx clock configurations remains challenging. Potential issues include misaligned PLL divider ratios and improper sysref signal routing, which can lead to synchronization errors. Therefore, to ensure coherent operation across all channels, it is necessary to carefully fine-tune the PLL settings and configure the sysref routing to maintain proper clock distribution [55]. This careful clock management is essential for enabling the high-fidelity performance required in IBFD systems.

IBFD System Measurement Setup

The block diagram of the integrated antenna-RFSoC measurement platform is shown in Figure 3.3. This setup combines the DACs, ADCs, programmable logic (PL), and processing system (PS) cores of the RFSoC ZCU216 device into a unified testbed. In order to simplify initial validation and maintain operation within the linear regime, no additional external PAs or LNAs are used in this configuration. The system is therefore assumed to operate linearly.

A movable probe antenna can be switched between two amplifiers: Amp1 or Amp2, each

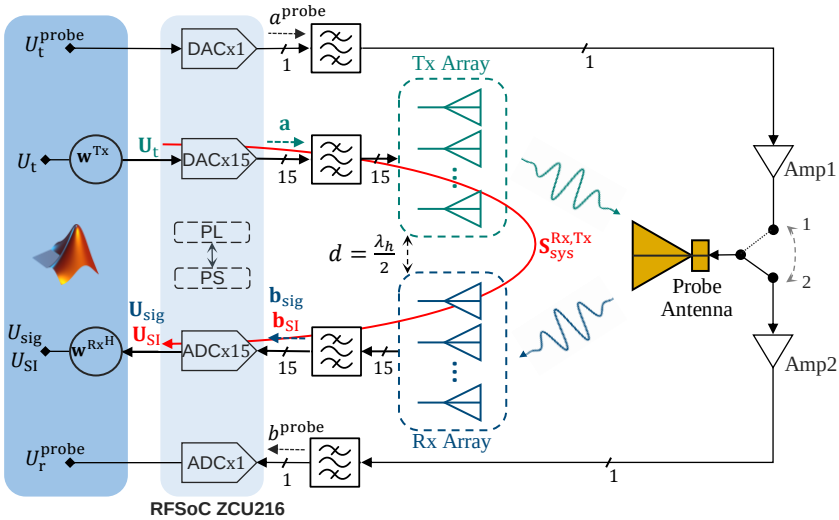

Figure 3.3: Block diagram of the integrated IBFD antenna system - RFSoC measurement platform. DACs generate transmit signals processed by the Tx array, while ADCs capture received signals at the Rx array. A probe antenna connected to either Amp1 or Amp2 is used for element characterization and coupling matrix measurements.

providing 50 dB gain to compensate for free-space propagation losses during measurements. Amp1 is typically used for reception and Amp2 for transmission, depending on the specific measurement step.

The measurement sequence begins with the generation of a discrete-time signal representing a continuous-wave tone at a carrier frequency ω_c. Although the Xilinx standard graphical user interface tools can generate basic waveforms, greater flexibility is achieved through an in-house MATLAB function that produces time-domain samples with optimized spectral purity (minimizing spurious content) [55]. The resulting digital signal is expressed as

$$g[n] = \mathfrak{Re}\{U_t e^{jn\omega_c/f_s}\}, \tag{3.1}$$

where $n \in \mathbb{Z}$ is the discrete time index, f_s is the DAC sampling frequency, and U_t is a complex phasor representing the signal amplitude and phase.

The complex phasor U_t is multiplied by the transmit beamforming vector $\mathbf{w}^{Tx}$ to form the 15×1 vector $\mathbf{U}_t$. These digital signals are converted to synchronized analog outputs $\mathbf{a} \propto \mathbf{U}_t$ via the DACs, passed through baluns, and incident onto the Tx antenna array.

At the receive side, the received analog waves, after passing through corresponding baluns, are captured by the ADCs and form two 15×1 vectors: $\mathbf{b}_{sig}$ (desired signal component) and $\mathbf{b}_{SI}$ (self-interference component). After digitization, the resulting signals $\mathbf{U}_{sig} \propto \mathbf{b}_{sig}$ and $\mathbf{U}_{SI} \propto \mathbf{b}_{SI}$ are processed by multiplying with the conjugate-transposed Rx beamforming vector $(\mathbf{w}^{Rx})^H$ to yield the final complex phasor outputs U_{sig} and U_{SI}.

All stages of signal generation, control, capture, and post-processing are performed within MATLAB, which interfaces with the RFSoC board. Frequency-domain analysis is performed using the Fast Fourier Transform applied to the acquired time-domain samples.

The complete measurement procedure consists of the following steps:

- **Tx EEP Measurements:** The probe antenna is connected to Amp2 via switch

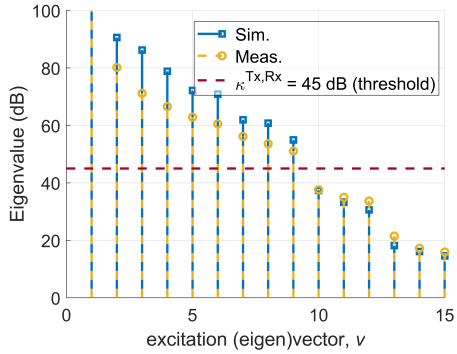

Figure 3.4: Simulation–measurement comparison: Eigenvalue spectrum of $[(\mathbf{S}_{\text{sys}}^{\text{Rx,Tx}})^{\text{H}}\mathbf{S}_{\text{sys}}^{\text{Rx,Tx}}]^{-1}$ at $f_c = 3.5$ GHz.

position 2. Each Tx array element is excited individually with a 1 V signal while the remaining elements are terminated. The received voltage $U_{\text{r}}^{\text{probe}}$ is recorded and is proportional to the Tx element's EEP.

- **Rx EEP Measurements:** Switching to position 1, the probe acts as the transmitter with $U_{\text{t}}^{\text{probe}} = 1$ V. The voltages measured at each Rx array element are proportional to the respective Rx element EEPs.

- **Coupling Matrix Measurement:** With the probe antenna turned off, each Tx array element is sequentially excited with a 1 V signal while the others remain terminated. The resulting voltages at the Rx array form the columns of the system coupling matrix $\mathbf{S}_{\text{sys}}^{\text{Rx,Tx}}$, defining the linear relationship:

$$\mathbf{U}_{\text{SI}} = \mathbf{S}_{\text{sys}}^{\text{Rx,Tx}}\mathbf{U}_{\text{t}}. \tag{3.2}$$

- **Beamformer Optimization:** Using the measured Tx EEPs and the system coupling matrix $\mathbf{S}_{\text{sys}}^{\text{Rx,Tx}}$, the Tx beamformer $\mathbf{w}^{\text{Tx}}$ is optimized according to the criteria in (2.7). For this optimization, it is assumed that $\mathbf{S}^{\text{Rx,Tx}} = \mathbf{S}_{\text{sys}}^{\text{Rx,Tx}}$ and that $\mathbf{a} = \mathbf{U}_{\text{t}}$ (proportionality constants cancel when evaluating power ratios). Subsequently, the Rx beamformer $(\mathbf{w}^{\text{Rx}})^*$ is optimized according to (2.8) to achieve the target residual SI suppression level.

3.2 Validation Results and Discussion

This section presents the validation of the proposed joint Tx-Rx beamforming strategy, described in Section 2.2, for an IBFD system operating at a center frequency of $f_c = 3.5$ GHz.

The eigenvalue spectrum, computed from both simulated and measured Tx-Rx coupling matrices, provides insight into the available degrees of freedom for optimizing the Tx beamformer $\mathbf{w}^{\text{Tx}}$. Figure 3.4 shows the eigenvalue spectrum of the matrix $[(\mathbf{S}_{\text{sys}}^{\text{Rx,Tx}})^{\text{H}}\mathbf{S}_{\text{sys}}^{\text{Rx,Tx}}]^{-1}$, where $\mathbf{S}_{\text{sys}}^{\text{Rx,Tx}}$ is either the simulated or the measured coupling matrix.

The number of dominant eigenvalues above a threshold of $\kappa^{\text{Tx,Rx}} = 45$ dB determines the effective number of degrees of freedom for beamforming optimization[2]. Good agreement

[2] A threshold of $\kappa^{\text{Tx,Rx}} = 45$ dB corresponds to a maximum available transmit power $P_{\text{av}} \approx 12$ dBm, as-

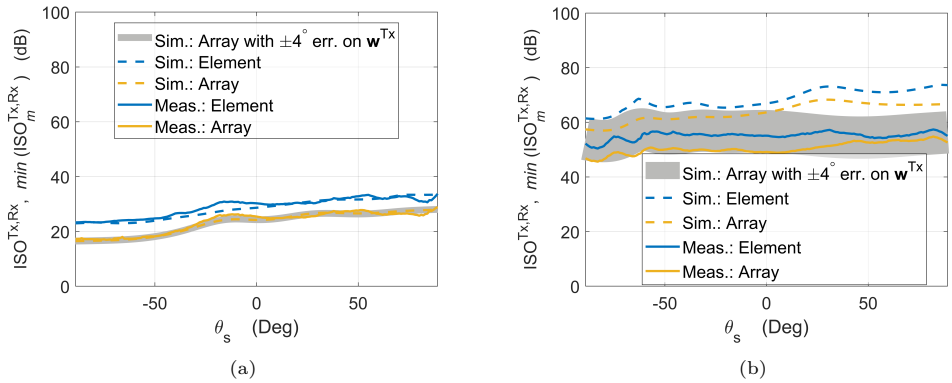

Figure 3.5: Simulation–measurement comparison of Rx array/element isolation over E-plane scan angles: (a) Using a conventional Tx maxGain beamformer; (b) Using the proposed Tx beamformer with $\kappa^{\mathrm{Tx,Rx}} = 45$ dB.

between the simulated and measured eigenvalue spectra is observed, particularly for lower-order eigenvalues associated with stronger coupling. Differences become more pronounced for higher-order eigenvalues corresponding to weaker coupling, mainly due to measurement noise and hardware imperfections.

Figure 3.5(a) illustrates the Rx array isolation achieved using a conventional Tx maximum-gain (maxGain) beamformer, where isolation levels between 17 and 27 dB are recorded. In contrast, the proposed Tx beamformer achieves Rx array isolation levels exceeding 45 dB, as shown in Figure 3.5(b).

Both simulation and measurement results exhibit small discrepancies at lower isolation levels, but significantly larger differences emerge at higher isolation levels. These discrepancies are attributed to hardware non-linearities introduced by the DACs. To quantify this effect, a random $\pm 4^\circ$ phase error was intentionally introduced into the Tx beamformer $\mathbf{w}^{\mathrm{Tx}}$ during simulations. As shown in Figures 3.5(a) and 3.5(b), minor isolation degradations are observed under phase errors. These degradations grow with higher isolation targets but remain within acceptable operational limits, demonstrating the robustness of the proposed beamforming method against realistic hardware impairments.

Figure 3.6(a) shows the normalized maximum Tx and Rx antenna gains over E-plane scan angles for both the conventional and the proposed beamforming approaches.

A slight discrepancy is observed between the simulated and measured Tx gains, particularly at positive scan angles. This is primarily attributed to the irradiation of ground plane edge absorbers in the measurement setup, an effect not accounted for in the simulation model. Additionally, a reduction in Tx antenna gain is noted at large negative angles (e.g., approximately 4.5 dB at -30°) when using the proposed beamformer compared to the conventional Tx maxGain beamformer. This degradation is due to the reduced number of usable excitation vectors that satisfy the isolation constraint $\kappa^{\mathrm{Tx,Rx}}$.

For the Rx beamforming demonstration, a residual SI suppression target of $\kappa_{\mathrm{SI}} = -80$ dBW is adopted, although the theoretical dynamic range of the system allows suppression down to approximately -100 dBW[3]. Notably, from prior analysis (Section 2.3), it was shown that κ_{SI}

suming the LNA 1 dB compression point with modulation-induced backoff is approximately -33 dBm.
[3] $P_{\mathrm{SI}} = |\Delta U_{\mathrm{SI}}|^2/(2 \cdot 50)$, where the ADC voltage resolution $\Delta U_{\mathrm{SI}} \approx 1/2^{14}$ V/bit.

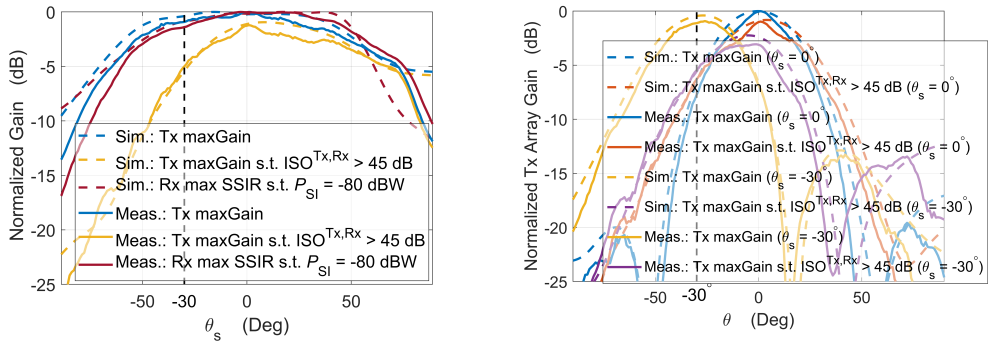

Figure 3.6: Simulation–measurement comparison: (a) Maximum Tx and Rx antenna gains achieved by the proposed joint Tx-Rx beamformer with $\kappa^{\mathrm{Tx,Rx}} = 45$ dB and $\kappa_{\mathrm{SI}} = -80$ dBW over E-plane scan angles; (b) Normalized Tx array radiation patterns at different E-plane scan angles.

levels up to −100 dBW impose little to no performance penalty on the beamforming gain. Discrepancies between simulation and measurement results for the Rx array gain at large negative angles are mainly attributed to the absorbers in the measurement setup, a factor not included in the simulation model. Conversely, at large positive angles, measurement accuracy is impacted by increased interference, as illustrated in Figure 3.6(a).

To further evaluate the beamforming performance, Tx array beam patterns were measured and simulated over E-plane scan angles ranging from −90° to 90° in 1° steps. Figure 3.6(b) illustrates the normalized maximum Tx array gain patterns at −30° and broadside. The proposed beamforming method results in a wider radiation pattern compared to the conventional Tx maxGain beamformer, reflecting the trade-off between beam directivity and achieving the stringent isolation constraint.

Figure 3.7 demonstrates the achieved total IBFD system isolation using the proposed joint Tx-Rx beamforming approach. The system consistently achieves isolation levels exceeding 80 dB. Minor measurement degradations are observed, which can be attributed to phase errors in the RFSoC DAC/ADC outputs, non-linear behavior of the converters, and the inherent limitations of the system's dynamic range.

Finally, the nonlinearities of the DAC/ADC chain are analyzed to better interpret the measurement results using the DAC-to-ADC loopback structure. The focus is on how amplitude and phase difference errors vary with the DAC input amplitude, $|V_{\mathrm{in}}|$, and phase, $\arg\{V_{\mathrm{in}}\}$.

Figure 3.8(a) shows the system response as $|V_{\mathrm{in}}|$ varies with a fixed input phase. The amplitude error, $\Delta|V_{\mathrm{out}}|$, exhibits weak nonlinearity, likely resulting from saturation or quantization effects. The corresponding phase error, $\Delta\arg\{V_{\mathrm{out}}\}$, swings between −1.5° and 1.5°, indicating high sensitivity to input amplitude.

Figure 3.8(b) presents the response to varying $\arg\{V_{\mathrm{in}}\}$ at a fixed amplitude. The amplitude error displays strong nonlinearity, reaching up to 80 mV. The phase error fluctuates between −3° and 3°, with sharp transitions highlighting the impact of input phase on nonlinear phase response.

These results demonstrate the complex nonlinear behavior of the DAC/ADC loopback structure, where both amplitude and phase responses are influenced by the input signal char-

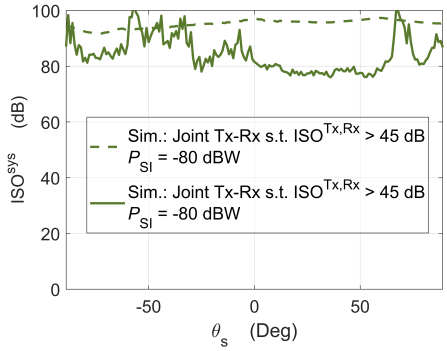

Figure 3.7: Simulation–measurement comparison: Total IBFD system isolation achieved with the proposed joint Tx–Rx beamformer.

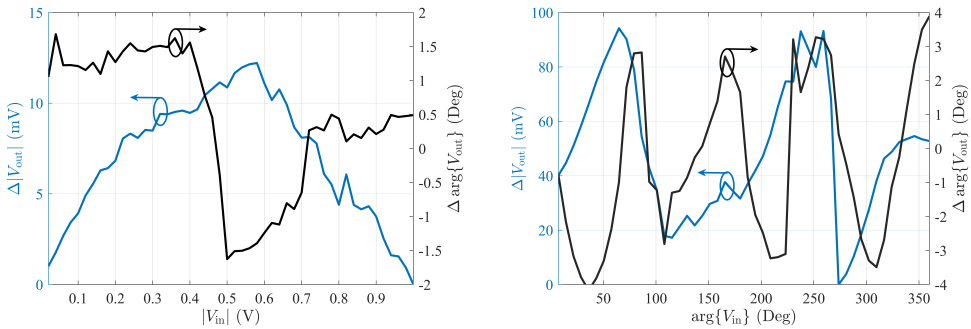

(a) (b)

Figure 3.8: $\Delta|V_{\text{out}}|$ and $\Delta \arg\{V_{\text{out}}\}$ at the ADC output for DAC-to-ADC loopback structure: (a) varying $|V_{\text{in}}|$ for fixed $\arg\{V_{\text{in}}\}$; (b) varying $\arg\{V_{\text{in}}\}$ for fixed $|V_{\text{in}}|$.

acteristics. Such nonlinearities can degrade measurement accuracy and must be considered in system design and calibration.

CHAPTER 4

Concluding Remarks and Future Work

A comprehensive mathematical framework was developed to formulate the joint Tx-Rx beamforming problem as a constrained optimization task for IBFD wireless systems. The proposed Tx beamforming strategy maximizes transmit array gain while ensuring that the coupled power at the Rx input remains below a critical threshold level, thereby preventing LNAs from operating in the nonlinear region. Beyond initial suppression at the Rx input, the proposed Rx beamforming method further reduces residual SI to a predefined level, enhancing SSIR and improving the receiver's ability to recover the desired signal.

The effectiveness of the framework was experimentally validated using a multi-tile RFSoC-based testbed, achieving high levels of system isolation and demonstrating the practical feasibility of the joint beamforming approach under realistic hardware conditions.

Several directions exist to extend this research:

- **Wideband Extension:** Extend the joint Tx-Rx beamforming framework to machine learning designed full-duplex antennas, and evaluate its performance over wideband and multi-carrier systems, where SI becomes frequency-selective. This will enable assessment under more realistic deployment conditions and support applications requiring broader spectral operation.

- **Nonlinear SI Modeling:** Extending the framework to incorporate nonlinear distortions from hardware impairments such as PAs, mixers, and DACs/ADCs.

- **SI Channel Estimation for Antenna Arrays:** Develop advanced SI channel estimation techniques tailored for IBFD antenna arrays, enabling more precise and adaptive beamforming solutions in dynamic environments.

- **Real-Time Adaptive Beamforming:** Integrating real-time environmental sensing to dynamically adapt Tx-Rx beamformers to environmental changes, enhancing performance in mobile or rapidly changing channels.

Together, these directions offer a clear path to enhancing the scalability and adaptability of proposed beamforming approach for IBFD systems. Ultimately, this work establishes joint Tx-Rx beamforming as a compelling and practical approach to tackling the fundamental

SI challenge in full-duplex wireless communication, bringing us closer to realizing high-performance, spectrally efficient, and adaptive wireless networks of the future.

CHAPTER 5

Summary of included papers

This chapter provides a summary of the included papers.

5.1 Paper A

Mustafa Ayebe, Johan Malmström, Sten E. Gunnarson, Henrik Holter, Marianna Ivashina, Carlo Bencivenni, Rob Maaskant
Systematic Self-Interference Mitigation In Full Duplex Antenna Arrays Via Transmit Beamforming
2023 International Conference on Electromagnetics in Advanced Applications (ICEAA), Venice, Italy, 2023.
©IEEE DOI: 10.1109/ICEAA57318.2023.10297706. .

The paper derives an optimal antenna array excitation vector to maximize array gain in a given direction, while limiting the coupling power to the receive side's low-noise amplifiers in in-band full-duplex systems. This approach reduces hardware complexity by allowing some interference, preserving freedom for transmit beamforming. Numerical results are shown for a 25-element transmit and receive setup with specific spacing.

5.2 Paper B

Mustafa Ayebe, Rob Maaskant, Johan Malmström, Sten E. Gunnarson, Henrik Holter, Marianna Ivashina
3D-printed Silver-coated Vivaldi Array With Integrated Coaxial Probe Feeding
2024 IEEE International Symposium on Antennas and Propagation and INC/USNC-URSI Radio Science Meeting (AP-S/INC-USNC-URSI),
Firenze, Italy, 2024.
©IEEE DOI: 10.1109/AP-S/INC-USNC-URSI52054.2024.10686495.

A Vivaldi antenna array for 3–6 GHz phased array applications is designed with a novel coaxial probe feed. Simulated active reflection coefficients stay below -10 dB for $\pm 60^\circ$ E-plane and $\pm 50^\circ$ H-plane scans. Measured results for a 1×5 array agree with simulations, validating the infinite array model and probe feed design. The 3D-printed, silver-coated fabrication enables rapid, cost-effective prototyping.

5.3 Paper C

Mustafa Ayebe, Rob Maaskant, Johan Malmström, Sten E. Gunnarson, Henrik Holter, Marianna Ivashina
Evaluation of the Self-Interference Cancellation Limits of Full-Duplex Antenna Arrays Using Zynq UltraScale+ RF System-On-Chip Board
2024 IEEE International Symposium on Phased Array Systems and Technology (ARRAY), Boston, MA, USA, 2024, pp. 1-4.

We present an experimental procedure using a state-of-the-art RFSoC to evaluate self-interference cancellation in full-duplex array antennas. Our study focuses on the system's ability to null self-interference under hardware imperfections and practical conditions. This assessment is essential for complex array transceivers involving non-linear components and advanced beamforming to enhance antenna gain, radiated power, and sensitivity while canceling interference. The setup includes a 1×5 Vivaldi antenna array operating in the 3–6 GHz band, connected to the RFSoC's digital transceiver. We introduce a calibration procedure that compensates for DAC errors and synchronizes transmit channels, achieving up to 63 dB cancellation.

5.4 Paper D

Mustafa Ayebe, Rob Maaskant, Johan Malmström, Sten E. Gunnarson, Marianna Ivashina, Henrik Holter
Joint Tx-Rx Beamforming for Optimal Gain and Self-Interference Mitigation in In-Band Full-Duplex Arrays: Theory, Figures of Merit, and Validation
IEEE Antennas and Wireless Propagation Letters (2025).

We present a joint transmit (Tx) and receive (Rx) beamforming method for in-band full-duplex antenna systems, addressing self-interference (SI) leakage and non-linear gain compression in the receiver's low-noise amplifiers (LNAs). Unlike conventional methods that handle Tx and Rx beamforming independently, our approach optimizes Tx gain while controlling SI at the LNA input to maintain linearity and further suppresses residual SI at the Rx output—validated using a commercial radio frequency system-on-chip evaluation board and a 3×5 Tx/Rx Vivaldi antenna array operating in the 3–6 GHz band.

5.5 Paper E

Mustafa Ayebe, Rob Maaskant, Marianna Ivashina, Johan Malmström, Sten E. Gunnarson, Henrik Holter, Simon Westergren, Erik Johansson
In-Band Full-Duplex Antenna Beamforming and Synchronization for Self-Interference Mitigation: Multi-Tile RFSoC Testbed Design and Deployment
2025 19th European Conference on Antennas and Propagation (EuCAP), Stockholm, Sweden, 2025. .

This paper presents an in-band full-duplex communication and sensing testbed using digital beamforming on the Xilinx ZCU216 RFSoC platform with 16 digital-to-analog converters and 16 analog-to-digital converters (14-bit) across four tiles. Key challenges include phase synchronization across RFSoC tiles and self-interference (SI) mitigation due to mutual coupling between transmit (Tx) and receive (Rx) antenna arrays. To address these, we used Tx beamforming for maximum gain and Rx beamforming to enhance the signal-to-SI ratio.

Our setup includes two 1×5 Vivaldi antenna arrays (3–6 GHz) and a multi-tile synchronization framework. Experimental results show over 80 dB SI suppression with half-wavelength spacing (@6 GHz) between Tx and Rx arrays, demonstrating the potential of the testbed for 6G communication and radar sensing.

References

[1] M. Mohammadi, Z. Mobini, D. Galappaththige, and C. Tellambura, "A comprehensive survey on full-duplex communication: Current solutions, future trends, and open issues," *IEEE Communications Surveys & Tutorials*, vol. 25, no. 4, pp. 2190–2244, 2023.

[2] D. Kim, H. Lee, and D. Hong, "A survey of in-band full-duplex transmission: From the perspective of phy and mac layers," *IEEE Communications Surveys & Tutorials*, vol. 17, no. 4, pp. 2017–2046, 2015.

[3] B. Smida, A. Sabharwal, G. Fodor, G. C. Alexandropoulos, H. A. Suraweera, and C.-B. Chae, "Full-duplex wireless for 6g: Progress brings new opportunities and challenges," *IEEE Journal on Selected Areas in Communications*, vol. 41, no. 9, pp. 2729–2750, 2023.

[4] H. Krishnaswamy and G. Zussman, "1 chip 2x the bandwidth," *IEEE Spectrum*, vol. 53, no. 7, pp. 38–54, 2016.

[5] B. Smida, R. Wichman, K. E. Kolodziej, H. A. Suraweera, T. Riihonen, and A. Sabharwal, "In-band full-duplex: The physical layer," *Proceedings of the IEEE*, 2024.

[6] B. Smida, R. Wichman, K. E. Kolodziej, H. A. Suraweera, T. Riihonen, and A. Sabharwal, "In-band full-duplex: The physical layer," *Proceedings of the IEEE*, vol. 112, no. 5, pp. 433–462, 2024.

[7] T. Wild, V. Braun, and H. Viswanathan, "Joint design of communication and sensing for beyond 5g and 6g systems," *IEEE Access*, vol. 9, pp. 30 845–30 857, 2021.

[8] D. K. P. Tan, J. He, Y. Li, *et al.*, "Integrated sensing and communication in 6g: Motivations, use cases, requirements, challenges and future directions," in *2021 1st IEEE International Online Symposium on Joint Communications & Sensing (JC&S)*, IEEE, 2021, pp. 1–6.

[9] H. Ju and R. Zhang, "Optimal resource allocation in full-duplex wireless-powered communication network," *IEEE Transactions on Communications*, vol. 62, no. 10, pp. 3528–3540, 2014.

[10] E. Lagunas, T. Ramirez-Parracho, J. A. Vasquez-Peralvo, *et al.*, "Full-duplex techniques for satellite communications: Feasibility analysis and roadmap," *IEEE Open Journal of the Communications Society*, 2025.

[11] A. Kiayani, M. Z. Waheed, L. Anttila, *et al.*, "Adaptive nonlinear rf cancellation for improved isolation in simultaneous transmit–receive systems," *IEEE Transactions on Microwave Theory and Techniques*, vol. 66, no. 5, pp. 2299–2312, 2018.

[12] D. Korpi, T. Riihonen, V. Syrjälä, L. Anttila, M. Valkama, and R. Wichman, "Full-duplex transceiver system calculations: Analysis of adc and linearity challenges," *IEEE Transactions on Wireless Communications*, vol. 13, no. 7, pp. 3821–3836, 2014.

[13] M. Duarte and A. Sabharwal, "Full-duplex wireless communications using off-the-shelf radios: Feasibility and first results," in *2010 Conference Record of the Forty Fourth Asilomar Conference on Signals, Systems and Computers*, IEEE, 2010, pp. 1558–1562.

[14] M. B. Dastjerdi, S. Jain, N. Reiskarimian, A. Natarajan, and H. Krishnaswamy, "Analysis and design of a full-duplex two-element mimo circulator-receiver with high tx power handling exploiting mimo rf and shared-delay baseband self-interference cancellation," *IEEE Journal of Solid-State Circuits*, vol. 54, no. 12, pp. 3525–3540, 2019.

[15] K. E. Kolodziej, B. T. Perry, and J. S. Herd, "In-band full-duplex technology: Techniques and systems survey," *IEEE Transactions on Microwave Theory and Techniques*, vol. 67, no. 7, pp. 3025–3041, 2019.

[16] E. Everett, A. Sahai, and A. Sabharwal, "Passive self-interference suppression for full-duplex infrastructure nodes," *IEEE Transactions on Wireless Communications*, vol. 13, no. 2, pp. 680–694, 2014.

[17] H. Nawaz and I. Tekin, "Compact dual-polarised microstrip patch antenna with high interport isolation for 2.5 ghz in-band full-duplex wireless applications," *IET Microwaves, Antennas & Propagation*, vol. 11, no. 7, pp. 976–981, 2017.

[18] M. Heino, S. N. Venkatasubramanian, C. Icheln, and K. Haneda, "Design of wave-traps for isolation improvement in compact in-band full-duplex relay antennas," *IEEE Transactions on Antennas and Propagation*, vol. 64, no. 3, pp. 1061–1070, 2015.

[19] S. N. Venkatasubramanian, L. Li, A. Lehtovuori, C. Icheln, and K. Haneda, "Impact of using resistive elements for wideband isolation improvement," *IEEE transactions on antennas and propagation*, vol. 65, no. 1, pp. 52–62, 2016.

[20] M. A. Elmansouri, A. J. Kee, and D. S. Filipovic, "Wideband antenna array for simultaneous transmit and receive (star) applications," *IEEE Antennas and Wireless Propagation Letters*, vol. 16, pp. 1277–1280, 2016.

[21] T. Snow, C. Fulton, and W. J. Chappell, "Transmit–receive duplexing using digital beamforming system to cancel self-interference," *IEEE Transactions on Microwave Theory and Techniques*, vol. 59, no. 12, pp. 3494–3503, 2011.

[22] M. Ayebe, R. Maaskant, J. Malmström, S. E. Gunnarson, H. Holter, and M. Ivashina, "Evaluation of the self-interference cancellation limits of full-duplex antenna arrays using zynq ultrascale+ rf system-on-chip board," in *2024 IEEE International Symposium on Phased Array Systems and Technology (ARRAY)*, IEEE, 2024, pp. 1–4.

[23] A. T. Wegener and W. J. Chappell, "Coupled antenna scheme using filter design techniques and tunable resonators to show simultaneous transmit and receive," in *2013 IEEE MTT-S International Microwave Symposium Digest (MTT)*, IEEE, 2013, pp. 1–4.

[24] J. I. Choi, M. Jain, K. Srinivasan, P. Levis, and S. Katti, "Achieving single channel, full duplex wireless communication," in *Proceedings of the sixteenth annual international conference on Mobile computing and networking*, 2010, pp. 1–12.

[25] D. Bharadia, E. McMilin, and S. Katti, "Full duplex radios," in *Proceedings of the ACM SIGCOMM 2013 conference on SIGCOMM*, 2013, pp. 375–386.

[26] M. Duarte, C. Dick, and A. Sabharwal, "Experiment-driven characterization of full-duplex wireless systems," *IEEE Transactions on Wireless Communications*, vol. 11, no. 12, pp. 4296–4307, 2012.

[27] M. Duarte, A. Sabharwal, V. Aggarwal, *et al.*, "Design and characterization of a full-duplex multiantenna system for wifi networks," *IEEE Transactions on Vehicular Technology*, vol. 63, no. 3, pp. 1160–1177, 2013.

[28] S. B. Venkatakrishnan, E. A. Alwan, and J. L. Volakis, "Wideband rf self-interference cancellation circuit for phased array simultaneous transmit and receive systems," *IEEE Access*, vol. 6, pp. 3425–3432, 2018.

[29] D.-J. van den Broek, E. A. Klumperink, and B. Nauta, "An in-band full-duplex radio receiver with a passive vector modulator downmixer for self-interference cancellation," *IEEE journal of solid-state circuits*, vol. 50, no. 12, pp. 3003–3014, 2015.

[30] Y. Liu, X. Quan, W. Pan, and Y. Tang, "Digitally assisted analog interference cancellation for in-band full-duplex radios," *IEEE Communications Letters*, vol. 21, no. 5, pp. 1079–1082, 2017.

[31] T. Riihonen, S. Werner, and R. Wichman, "Mitigation of loopback self-interference in full-duplex mimo relays," *IEEE transactions on signal processing*, vol. 59, no. 12, pp. 5983–5993, 2011.

[32] D. Korpi, L. Anttila, V. Syrjälä, and M. Valkama, "Widely linear digital self-interference cancellation in direct-conversion full-duplex transceiver," *IEEE Journal on Selected Areas in Communications*, vol. 32, no. 9, pp. 1674–1687, 2014.

[33] D. Korpi, L. Anttila, and M. Valkama, "Reference receiver based digital self-interference cancellation in mimo full-duplex transceivers," in *2014 IEEE Globecom Workshops (GC Wkshps)*, IEEE, 2014, pp. 1001–1007.

[34] K. Komatsu, Y. Miyaji, and H. Uehara, "Frequency-domain hammerstein self-interference canceller for in-band full-duplex ofdm systems," in *2017 IEEE Wireless Communications and Networking Conference (WCNC)*, IEEE, 2017, pp. 1–6.

[35] H. Krishnaswamy and L. Zhang, "Analog and rf interference mitigation for integrated mimo receiver arrays," *Proceedings of the IEEE*, vol. 104, no. 3, pp. 561–575, 2016.

[36] B. P. Day, A. R. Margetts, D. W. Bliss, and P. Schniter, "Full-duplex bidirectional mimo: Achievable rates under limited dynamic range," *IEEE Transactions on Signal Processing*, vol. 60, no. 7, pp. 3702–3713, 2012.

[37] X. Huang and J. Guo, "In-band full-duplex technology for future generations of wireless communications," UTS: Global Big Data Technologies Centre, White Paper, Nov. 2021, Contact: Professor Xiaojing Huang, Distinguished Professor Jay Guo.

[38] T. Chen, M. B. Dastjerdi, H. Krishnaswamy, and G. Zussman, "Wideband full-duplex phased array with joint transmit and receive beamforming: Optimization and rate gains," in *Proceedings of the Twentieth ACM International Symposium on Mobile Ad Hoc Networking and Computing*, 2019, pp. 361–370.

[39] J. P. Doane, K. E. Kolodziej, and B. T. Perry, "Simultaneous transmit and receive performance of an 8-channel digital phased array," in *2017 IEEE International Symposium on Antennas and Propagation & USNC/URSI National Radio Science Meeting*, IEEE, 2017, pp. 1043–1044.

[40] K. E. Kolodziej, B. T. Perry, and J. S. Herd, "Simultaneous transmit and receive (star) system architecture using multiple analog cancellation layers," in *2015 IEEE MTT-S International Microwave Symposium*, IEEE, 2015, pp. 1–4.

[41] N. Honma, M. Tsunezawa, Y. Yamamoto, and Y. Kashino, "Realizing in-band full-duplex mimo with feasible rf-chain: Key challenges," in *2017 IEEE Conference on Antenna Measurements & Applications (CAMA)*, IEEE, 2017, pp. 284–287.

[42] L. Lei, N. Saba, and S. G. Razul, "A multichannel self-interference cancellation prototyping system," in *2019 IEEE 2nd 5G World Forum (5GWF)*, IEEE, 2019, pp. 427–432.

[43] E. Everett, C. Shepard, L. Zhong, and A. Sabharwal, "Softnull: Many-antenna full-duplex wireless via digital beamforming," *IEEE Transactions on Wireless Communications*, vol. 15, no. 12, pp. 8077–8092, 2016.

[44] M. B. Dastjerdi, N. Reiskarimian, T. Chen, G. Zussman, and H. Krishnaswamy, "Full duplex circulator-receiver phased array employing self-interference cancellation via beamforming," in *2018 IEEE Radio Frequency Integrated Circuits Symposium (RFIC)*, IEEE, 2018, pp. 108–111.

[45] M. Ayebe, R. Maaskant, S. E. Gunnarson, J. Malmström, M. Ivashina, and H. Holter, "Joint tx-rx beamforming for optimal gain and self-interference mitigation in in-band full-duplex arrays: Theory, figures of merit, and validation," *IEEE Antennas and Wireless Propagation Letters*, 2025.

[46] K. Kurokawa, "Power waves and the scattering matrix," *IEEE transactions on microwave theory and techniques*, vol. 13, no. 2, pp. 194–202, 1965.

[47] K. F. Warnick, D. B. Davidson, and D. Buck, "Embedded element pattern loading condition transformations for phased array modeling," *IEEE Transactions on Antennas and Propagation*, vol. 69, no. 3, pp. 1769–1774, 2020.

[48] H. van Trees, *Optimum array processing: Part IV of detection, estimation, and modulation theory*. John Wiley & Sons, 2002.

[49] M. Ayebe, J. Malmström, S. E. Gunnarson, *et al.*, "Systematic self-interference mitigation in full duplex antenna arrays via transmit beamforming," in *2023 International Conference on Electromagnetics in Advanced Applications (ICEAA)*, 2023, pp. 158–163.

[50] R. Maaskant, "Analysis of large antenna systems," Ph.D. dissertation, TUE, 2010.

[51] M. Ayebe, R. Maaskant, J. Malmström, S. E. Gunnarson, H. Holter, and M. Ivashina, "3d-printed silver-coated vivaldi array with integrated coaxial probe feeding," in *2024 IEEE International Symposium on Antennas and Propagation and INC/USNC-URSI Radio Science Meeting (AP-S/INC-USNC-URSI)*, 2024, pp. 7–8.

[52] M. Ayebe, "Design of vivaldi antenna operating in two frequency bands with distinct polarizations," M.S. thesis, OZU, 2023.

[53] N. R. Dusari and M. Rawat, "Practical implementation challenges in mimo beamforming and its applications," *IEEE Microwave Magazine*, vol. 26, no. 4, pp. 59–75, 2025.

[54] AMD Xilinx, *Zynq ultrascale+ rfsoc rf data converter v2.6 gen 1/2/3/dfe*, `https://docs.amd.com/r/en-US/pg269-rf-data-converter`, Accessed: 2025-04-19, Oct. 2022.

[55] M. Ayebe, R. Maaskant, M. Ivashina, *et al.*, "In-band full-duplex antenna beamforming and synchronization for self-interference mitigation: Multi-tile rfsoc testbed design and deployment," in *2025 19th European Conference on Antennas and Propagation (EuCAP)*, 2025.